Development and Validation of a 3-channel Optimal Estimation Cloud Top Effective Radius and Optical Thickness Retrieval

By
Kyle J. Leesman and Graeme L. Stephens

Department of Atmospheric Science
Colorado State University
Fort Collins, Colorado

Research was supported by the CloudSat Mission on NASA Cotnract: NAS5-99237

Colorado State University

Department of Atmospheric Science

Paper No. 784

ABSTRACT

DEVELOPMENT AND VALIDATION OF A 3-CHANNEL OPTIMAL ESTIMATION CLOUD TOP EFECTIVE RADIUS AND OPTICAL THICKNESS RETRIEVAL

The radiative influence of clouds is one of the most important and uncertain factors governing the global energy balance, however, the exact magnitude and sign of these changes is still a point of contention. The magnitude of the radiative effect has been shown to be a complicated function of cloud amount, cloud height, vertical distribution, location, and microphysical characteristics. The goal of this thesis is to develop an efficient, research-grade optimal estimation (OE) retrieval that seeks to determine these very characteristics of the global cloud population.

The OE retrieval was used to process a number of case studies with data from the Moderate Resolution Imaging Spectroradiometer (MODIS), as well as a subset of 2 months of data from the Visible and Infrared Scanner (VIRS), to develop spatial means and large scale histograms of retrieved cloud height, optical thickness, and cloud top particle effective radius.

Comparisons with the MODIS operational retrieval for water clouds show excellent agreement with optical thickness, characterized by discrepancies of less than 10%. While the OE effective radius retrievals exhibit a 10-45% low bias relative to the MODIS solution. This bias is shown to be reduced in ice cloud cases. However, these comparisons contain significant scatter due to the increased difficulty of the ice phase retrieval.

Joint histograms of retrieved cloud top height and optical thickness are shown to compare favorably to the International Satellite Cloud Climatology Project (ISCCP) data

in both the Tropical Rainfall Measurement Mission (TRMM) region, as well as a smaller Tropical West Pacific zone.

Precipitating water clouds were shown to have significantly larger median particle sizes than non-precipitating scenes. In addition, in non-raining cases effective radius and optical thickness appear uncorrelated, whereas in precipitating cases a positive correlation is found.

Spatial distributions of retrieved effective radius show robust negative correlations with observed aerosol optical thickness values. This effect is most pronounced in the Southern Ocean where seasonal variations in non-manmade aerosols are shown to result in a 20-30% reduction in cloud top effective radius in January relative to July. This seasonal variance is in excellent agreement with in-situ measurements taken during the Southern Ocean Cloud Experiment (SOCEX), the MODIS operational product does not contain this signal.

ACKNOWLEDGEMENTS

There are several people without whom this study could not have been performed. First and foremost, we would like to thank Dr. Philip Gabriel whose considerable time, effort, insight, teaching, and guidance were absolutely invaluable. In addition, thanks go to all of those in the Stephens' research group for their help and support of all sorts, but specifically: Sue Lini, Ian Whittmeyer, Todd Ellis, Tristan L'Ecuyer, Steve Cooper, Shanna Pitter, and Laurent Labonnet.

TABLE OF CONTENTS

LIST OF FIGURES

LIST OF TABLES

CHAPTER 1: INTRODUCTION

1.1 Importance of Cloud Microphysical Properties

The radiative influence of clouds is one of the most important and uncertain factors governing the global energy balance, and ultimately global climate change. Though it has been known for some time that clouds are strong modulators of the shortwave and longwave radiation budgets of the atmosphere (Ramanathan 1987; Ramanathan et al. 1989), the exact magnitude, and indeed the sign of the modulating effects of clouds remain as important points of contention in the atmospheric science community.

Studies by a large number of investigators over the past two decades have determined that the net radiative influence of clouds is a complicated function of cloud amount, vertical distribution, location, morphology, and microphysical characteristics. The role of the vertical distribution of clouds on the global radiation balance was elucidated by Cess (1989) and the debate was once again stirred in 2002 by (Lindzen 2002). Global Circulation Model (GCM) simulations of clouds have supported these theoretical studies by identifying cloud amount and the vertical distribution of clouds in the atmosphere as among the most important parameters to which the atmospheric energy balance is most sensitive (Weatherald and Manabe 1988; Chen and Ramaswary 1996)

Further, the effects of clouds on the energy balance are not static in time. As CO_2 concentrations in the atmosphere rise due to industrial and automotive emissions, there is a redistribution of energy in the atmospheric column. It is thought that this will lead to a potential increase in the global cloud amount due to changes in sea surface temperatures that may lead to increased low level atmospheric water vapor (Ramanathan 1981). In addition, this redistribution of energy may lead to a redistribution of clouds in the vertical.

The anthropogenic effects on clouds do not stop there, as was shown by (Twomey 1980). Increases in the aerosol concentration in the atmosphere affect the microphysical properties of clouds and, in turn, their radiative influence. Increases in aerosol concentration lead to increases in the albedo of low water clouds, referred to as the Twomey Effect. In addition, increases in low-level cloud condensation nuclei (CCN) concentrations are thought to reduce the prevalence of drizzle and the precipitation efficiency of maritime clouds. It is thought that these changes in amount, distribution, and optical properties of clouds will act as a feedback mechanism of sorts in response to the effects of increases in greenhouse gases. For example, increases in total global cloud amount would increase the effective albedo of the earth-atmosphere system, which would act to cool the planet. The vertical distribution of these cloud amount changes is also of central interest since increases in high cloud amount would have a more dramatic effect on the terrestrial infrared energy balance that low clouds. This is due to the fact that low level clouds have similar radiating temperatures to the surface, while cirrus clouds are significantly colder, leading to a sharply reduced value of outgoing longwave radiation.

The importance of characterizing the distribution and microphysical properties of clouds for the purposes of understanding their climate feedback role has come to the forefront of the atmospheric community and has led to a large number of satellite programs in recent years. Satellite platforms and instruments such as the Advanced Very High Resolution Radiometer (AVHRR), the series of Geostationary Operational Environmental Satellites (GOES), the Moderate Resolution Imaging Spectroradiometer (MODIS), and the Tropical Rainfall Measurement Mission (TRMM) have already yielded a wealth of valuable data in spectral regions (ie. visible, infrared, and microwave) important for the study of cloud microphysical properties. With the launch of CloudSat it will be possible to obtain the vertical profile of cloud microphysical properties through its millimeter band cloud profiling radar (CPR).

Observations of the global distribution of cloud amount, the vertical profile of clouds, and their microphysical properties are key to understanding the wider global climate change problem.

1.2 Microphysical Retrieval Background

The remote sensing literature is replete with methods of retrieving cloud top particle size and optical depth. Many of these methods are variations of the seminal works of Twomey and Cocks (1982) and Nakajima and King (1990) in which the optical properties of water clouds were determined though a reflectance mapping procedure. That method employs measurements from two channels: a channel of non-absorbing visible wavelengths (centered at 0.64 microns) that is primarily sensitive to

optical depth alone, and a channel of absorbing wavelengths in the near infrared (such as centered at 2.13 microns) that is sensitive to both optical depth and particle size. Their simple 2-channel look up table method has been expanded and refined by selected investigators through the years (e.g. Rolland et al. 2000), but the basic philosophy for daytime retrievals of using visible and near-infrared radiances remains popular.

Other methods that have been developed for nighttime retrievals use two infrared channels that exhibit slightly different radiative properties typically at wavelengths near 11 and 12 micrometers. These methods, however, are useful only for certain cloud types, primarily thin cirrus clouds (e.g. Platt 1973).

Methods of solving the inverse problem have included: constrained non linear least squared minimization (Worden et al. 1999), neural networks (Juliette and Clerbaux, 1999), principal component analysis (Tanre et al. 1996), Bayesan Monte-Carlo methods for non-Gaussian inverse problems (Tamminen and Kryola, 2001), bi-directional mapping techniques (Rolland et al. 2000), regularization methods (Eriksson, 2000), and discrepancy principals that extend regularization methods (Li and Huang, 1999).

The current study employs a 4 channel approach that, in addition to the Nakajima and King channel selection, has added a second near-IR channel near 3.7 microns, that is highly sensitive to particle size, and at a thermal IR channel near 11 microns that provides information pertaining to cloud phase and cloud height determination. The retrieval philosophy follows the optimal estimation framework introduced by Rodgers (1976) which minimizes a cost function through an iterative technique, that

uses Gaussian statistics to return the most probable cloud properties with explicit error characterization.

1.3 Nature of Study

The goal of this thesis is (i) to develop and to test an efficient research grade algorithm, (ii) to apply this algorithm to the Visible and Infrared Scanner (VIRS), a 5-channel passive space-borne radiometer that flies aboard the Tropical Rainfall Measurement Mission (TRMM) satellite that was launched in 1997, (iii) to contrast the results of these retrievals against results from other satellite instruments, most notably MODIS as well as with the International Satellite Cloud Climatology Project (ISCCP) program, and (iv) to examine the relationship between the microphysical properties obtained and precipitation measurements from the other TRMM sensors. Thus the retrieval algorithm developed here for the VIRS is potentially powerful since it can be adapted to use other observational instruments on the TRMM platform, For example, the TRMM platform contains a Microwave Imager (TMI) that is used to estimate rainfall as well as cloud liquid water path. The latter is a completely independent data test bed against which the VIRS LWP optical estimation retrieval can be compared and even integrated with the algorithms of this thesis, both subjects for future research. Further classifications and comparisons of retrieved optical quantities with rainfall are performed using the Precipitation Radar (PR), an active microwave system also on board TRMM. In addition to the other instruments on board, the data produced by TRMM's 7-year mission has provided a valuable

climatology of cloud properties, in the tropics and sub-tropics. Through 2004, the VIRS instrument is closing in on half a trillion cloud scene observations.

1.4 Outline and Principal Findings

Chapter 2 describes the retrieval methodology in detail, including the radiative transfer solver, the optimal estimation approach, and the assumptions about key model parameters such as the scattering phase function characterization.

Chapter 3 presents comparisons of the current retrieval adapted to use MODIS radiances as input with the actual MODIS operational retrieval. We first note that there are 3 different operational cloud property sets derived by MODIS. Generally good agreement was found with between the optimal estimation retrieved microphysical properties and the operational MODIS products, but with somewhat smaller top particle sizes obtained in the (OE) approach.

Chapter 4 examines the application of the algorithm to 2 months of a sampled VIRS data set for the purpose of compiling statistics over the global tropics. Statistical histograms of cloud height and optical thickness compared favorably with similar histograms available from the International Cloud Climatology Satellite Project (ISCCP) data, however the OE retrieval characterized fewer deep convective scenes and more optically thin high clouds than found by the ISCCP team. More detailed optical thickness/cloud top height distributions for ice clouds exhibited a robust tri-modal optical thickness structure, representing cirrus, thick cirrus, and deep convective clouds, in both the Tropical West Pacific (TWP) as well as the broader TRMM region. The 3 optical thickness regimes were found to have distinct particle

size distributions. Cirrus clouds had typical effective diameter values of 20-70 microns, with a median value near 45, while the thicker ice clouds were characterized by larger sizes and a more narrow size distribution centered near 55 microns. Precipitating clouds, as determined by the Precipitation Radar (PR), exhibited a very distinct effective radius histogram from non-precipitating scenes, with a median value of nearly 20 microns for warm raining clouds and roughly 13 microns for warm non-raining scenes. Maps of retrieved effective radii for water clouds from the OE VIRS retrieval exhibit similar large-scale structure to the operational MODIS data, but estimate somewhat smaller particles and contain larger zonal and seasonal variations. The fundamental cause of these retrieval discrepancies remains an open question. In addition, retrieved cloud top particle sizes show excellent negative correlations with aerosol optical thickness values. This effect is most pronounced in the Southern Ocean where seasonal variations in non-anthropogenic aerosols are shown to result in a 20-30% reduction in cloud top effective radius in January relative to July. This large seasonal effective radius reduction agrees very well with in-situ measurements made during the Southern Ocean Cloud Experiment (SOCEX) campaign over a small region of the Southern Oceans; this seasonal signal is not present in the operational MODIS data. Finally, expanding on the work of Nakajima and Nakajima (1995), regressions of optical thickness with effective radius are presented and used to identify a number of regions dominated by distinct water cloud modes, including aerosol influenced water clouds in which there was no drizzle mode, vertically developed precipitating clouds in pristine tropical environments, and an optically thin precipitating mode in regions of very clean boundary layer air.

Chapter 5 summarizes and concludes and presents a road map for future research.

CHAPTER 2: CLOUD PROPERTY RETRIEVAL SCHEME

2.1 Fundamentals of the Cloud Property Retrieval

The basis of the inversion approach rests on the work of Rodgers (1976,1990) and Marks and Rodgers (1993). These papers outline the optimal estimation mathematical framework for solving general inverse problems used here and in an increasing number of atmospheric science applications.

The inverse problem in this application is a method of inferring atmospheric states that are not directly observed through the use of a series of measurements and a model that physically relates these measurements to the atmospheric variables of interest.

Mathematically, the problem can be expressed as:

$$y = F(x,b) + \varepsilon_y \qquad (2.1)$$

where F is the forward model, in our case a radiative transfer model. The forward model relates the inferred atmospheric state, comprised of both assumed (b) and retrieved (x) components, to the observations used in the retrieval (y). The measurement error, ε_y, present in any observational platform must be considered if retrieval errors are to be meaningful. The retrieval is then a matter of selecting the appropriate state vector (x), in our retrieval the cloud optical thickness and cloud top effective radius, that minimizes the difference between the observations (y) and our forward model simulated observations F(x,b). Since the forward model is computationally expensive the optimal estimation framework developed by Rodgers

et al. is employed in order to perform state vector (x) selection as efficiently and objectively as possible.

The optimal estimation method is framed around Bayes' Theorem and Gaussian statistics to calculate the most likely atmospheric state vector associated with the provided measurements and *a priori* estimate. The Bayesian method uses *a priori* information, the forward model, and its associated Gaussian errors to find the most likely *a posteriori* state of the atmosphere. Gaussian statistics are utilized in reverence to the maximum ignorance principal since Gaussian errors introduce the least assumed information into the solution. The most probable solution is found by minimizing a quadratic cost function given by:

$$J = (x - x_a)^T S_a^{-1}(x - x_a) + (y - F(x,b))^T S_y^{-1}(y - F(x,b)) \qquad (2.2)$$

Here, the *a priori* state, x_a, and the associated error covariance matrix, S_a, characterize the *a priori* information. For our application, the two state variables, optical depth and effective radius, are considered independent, that is to say they have no covariance. In this case the S_a matrix becomes diagonal with each element representing the variance of the associated x_a value. The *a priori* information is added to the retrieval process to constrain the solution to physically realistic values. In the current application the *a priori* errors are assumed to be very large, therefore the x_a value only influences the retrieved solution to a significant degree in cases where the radiance has very little sensitivity to the retrieved values (i.e. very large optical depth or very small particles) In many applications the *a priori* value can be of principal importance since the state vector solution is often not unique in such highly non-linear systems; therefore an

appropriate *a priori* understanding constrains the retrieved state vector to the most likely of several physically consistent solutions.

The matrix Sy represents the uncertainty of both the sensor and the ability of our forward model to reproduce these observations accurately. The sensor and model uncertainties are independent and thus additive:

$$S_y = S_{yobs} + S_{ymodel} \quad (2.3)$$

The instrumental errors are documented to be on the order of 2% in the longwave and 6-9% in the shortwave for the VIRS instrument, while the MODIS instrument exhibits errors of 1-5% in all channels. The forward model calculations introduce many potential sources of error. Errors may exist in mathematics or physics of the forward model itself. However, due to the impressive agreement found between the RADIANT radiative transfer solution and other transfer codes, this uncertainty is considered negligible. A more important source of error is uncertainties associated with model input parameters such as errors in the assumed temperature and moisture profiles, and surface albedo assumptions. In addition, there are errors in the forward model itself due to incorrect assumptions regarding the scattering phase function (a function of the droplet size distribution) and deviations from a plane parallel atmosphere. Radiance errors associated with typical uncertainties in temperature and moisture profiles, droplet size distributions, and surface albedo were found to total 1-2% at .65 microns and 1.6 microns and 6-8% at 3.7 microns for water clouds (L'Ecuyer et al. 2004). The radiance uncertainty associated with the 3-dimensional structure of clouds was not considered in the L'Ecuyer study but is thought to be potentially significant. With this in mind observations at relatively small solar and

view angles are used in this study in an effort to minimize the highly uncertain effects of shadowing and cloud geometry. Taking all of these effects into account, it is clear that the errors can be extreme in individual cases. However, for this study a best guess standard deviation for the radiance uncertainty is employed.

Based on the uncertainty characterization presented above and an admittedly conservative assumption of radiance errors associated with cloud 3D structure, a S_y value of 5% of the measured radiance is applied in the visible and near-IR channels, while 10% is used for the 3.7 micron channel for water clouds using the MODIS instrument. For the VIRS instrument, 10% and 15% of measured radiances are assigned to S_y in the visible and shortwave-IR channels respectively, a result of the less precise instrument calibration associated with this platform. For ice clouds, somewhat larger errors are applied, due primarily to large potential errors in the scattering phase functions. The scattering phase function errors in ice clouds are both large and uncertain due to the kaleidoscope of crystal shapes that can occur in ice cloud layers. For these cases, errors of 20% are estimated in the visible and 1.6 microns channels, while a more conservative 30% error is considered typical in the 3.7-micron channel for both platforms. Though it is hard to imagine that forward model errors in each channel are completely independent since they are influenced by many of the same model assumptions, the degree to which they are correlated is hard to quantify and is therefore set to zero, resulting in a diagonal S_y matrix. It is found through sensitivity analysis that as long as the error correlation is relatively small that this omission results in negligible effects on the total errors of the retrieval.

The cost function J can be minimized via an iterative solution given by:

$$x^{i+1} = (S_a^{-1} + K^T S_y^{-1} K)^{-1} [S_a^{-1} x_a + K^T S_y^{-1} (y - F(x^i) + Kx^i)] \quad (2.4)$$

where K represents the partial derivative of the forward model with respect to the current iteration's state vector, that is the sensitivity of the modeled observations to each retrieved quantity.

$$K = \frac{\partial F(x^i, b)}{\partial x^i} \quad (2.5)$$

The method further defines an error covariance matrix, Sx, defined as:

$$S_x = (S_a^{-1} + K^T S_y^{-1} K)^{-1} \quad (2.6)$$

which is dependant on both *a priori* and model errors as well as the sensitivity of the radiance to the state parameters and provides a basis for determining explicit error bars on the retrieved quantities. For water cloud retrievals, typical errors in the particle size are found to be 10-15% for the MODIS instrument, and 15-20% for the VIRS, while typical uncertainties in the optical thickness range from 2-4% for the MODIS and 3-6% for the VIRS. In ice clouds, typical optical thickness errors are nearly 10%, while particle size errors are generally 30-40%.

The iteration (2.3) is considered converged when (e.g Marks and Rodgers 1993):

$$\Delta x^T S x^{-1} \Delta x \ << n \quad (2.7)$$

Where $\Delta x = x^{i+1} - x^i$ and n is the number of dimensions of the state vector, n =2 for our retrieval.

2.2 The Forward Model

The radiative transfer code employed as the retrieval's forward model, is the *Radiant* version 2.0 code developed at Colorado State University (Gabriel and Christi 2004). *Radiant*, in it's current form, is a multi-stream, 18-layer, plane-parallel,

radiative transfer solution that accounts for multiple scattering. It utilizes an eigen-matrix solution method (e.g. Benedetti et al. 2001) that contains the best characteristics of the more popular eigen-matrix and adding/doubling approaches which seeks to improve computational efficiency with no loss of accuracy. Its solutions have been compared to the radiance tables of Van de Hulst (1980) and with the Discrete Ordinate Method of Radiative Transfer (DISORT) solution with excellent agreement.

The basis of the radiative transfer theory that defines the forward model is described by the equation:

$$\mu \frac{dI(z,\mu,\phi)}{dz} = -\sigma_e(z) I(z,\mu,\phi) + \frac{\sigma_s(z)}{4\pi} \int_0^{2\pi} \int_{-1}^{1} P(z,\mu,\phi,\mu',\phi') I(z,\mu',\phi') d\mu' d,\phi' + \frac{F_\oplus}{4\pi} \sigma_s(z) P(z,\mu,\phi,\mu_\oplus,\phi_\oplus) e^{-\sigma_e(z_T - z)/\mu_\oplus} + \sigma_a(z) B(T(z)) \qquad (2.8)$$

Where, I is the radiance, μ and φ are the zenith and azimuth angles, z is an incremental height, σ_a, σ_s, and σ_e are the absorption, scattering and extinction coefficients, P is the scattering phase function, F is the incident solar flux, and B(T) is the Planck blackbody function.

The LHS describes the change in radiance (I) as it traverses an incremental atmospheric distance (dz). This quantity is modified by 4 physically distinct terms as given in the RHS. The first term describes the attenuation of the direct beam by absorption and out-scattering as it passes through the volume, components (a) and (b) in figure (2.1). Term two is a diffusive scattering source term that accounts for radiation from all other angles that is scattered into the direction of interest,

represented by process (c). The third term is a special case of the second in which the angle of the sun is considered separately from all other diffuse angles (d). Here the direct solar beam component that is scattered into the direction of interest appears as a source. The final source term accounts for the thermal emission over the incremental atmospheric distance being considered (e). The direct beam radiation that is unaffected by traversing the incremental distance of interest is represented by (f).

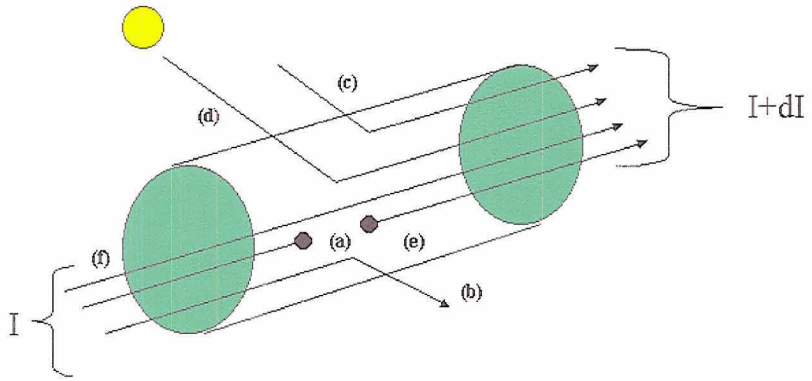

Figure 2.1: Conceptual model of the terms of the radiative transfer equation. a) Absorption b) Out-scattering c) Diffuse in-scattering d) Solar in-scattering e) Emission f) Transmission

The radiative calculations use temperature and moisture profiles taken from the NCEP re-analysis product matched to instrument footprint and interpolated to the 18 model layers. The retrieval using both the MODIS and VIRS measurements are performed using 4 channels, the characteristics of which are described in Table 2.1

2.3 Scattering Phase Functions for Water Clouds

There are three parameters in (2.7) that define the scattering properties of a radiative transfer code, the single scattering albedo (ω_o), the scattering phase function $P(\mu,\mu')$, and the cloud optical thickness (τ). Each of these is a function of the wavelength of radiation, particle size distribution, and the real and imaginary indices of refraction of the scattering particles, which are defined distinctly for each model layer. The single scatter albedo is a parameter that determines the fraction of radiation that is extinguished in a volume by scattering as opposed to both scattering and absorption. This quantity, along with the optical thickness defines the total energy that is scattered in the layer since:

$$\tau = \sigma_{ext} * ds \qquad (2.9) \qquad \sigma_{ext} = \sigma_{sca} + \sigma_{abs} \quad (2.10) \qquad \omega_o = (\sigma_{sca}) / (\sigma_{ext}) \quad (2.11)$$

Where, σ_{ext}, σ_{sca}, and σ_{abs} are the extinction, scattering and absorption coefficients and ds is the path length that the radiation travels.

Table 2.1: Channels used in the retrieval scheme

MODIS Channels

Channel	λ(microns)	$g_0(r_e = 10\mu)$	ω_0	Solar Flux(W/m^2)
1	0.62-0.67	.858	1.00	78.01
6	1.628-1.652	.841	.9944	5.60
20	3.66-3.84	.795	.9082	1.97
31	10.78-11.28	.924	.4251	0.00

VIRS Channels

Channel	λ(microns)	$g_0(r_e = 10\mu)$	ω_0	Solar Flux(W/m^2)
1	0.57-0.67	.860	1.00	168.16
2	1.57-1.65	.842	.9935	19.86
3	3.63-3.97	.795	.9067	3.607
4	10.23-11.27	.924	.4838	0.00

Once it is determined how much radiation is scattered within a model volume it is necessary to consider how this energy is redistributed. In the real atmosphere, this energy is scattered in all directions in a 3 dimensional sense by particles of all shapes and sizes. Theoretical and practical limitations on our model limit us to the assumption that the atmosphere is plane-parallel, that is uniform in the x and y directions. This limits us to producing phase functions that are only a function of zenith angle relative to the direction of incidence. Further, since we are most interested in studying water clouds we are assuming that the scattering is performed by spherical water droplets, a very good assumption for our sizes of interest, say (5 – 50 microns in radius). For ice clouds, a mix of ice particle morphologies is used in the range 10– 180 microns in diameter.

Many methods have been developed for estimating the actual scattering phase functions of particles. One common approximation is the Henyey-Greenstein (HG) phase function. This gross estimate is based on a single parameter, the asymmetry

parameter (g). The asymmetry parameter is a function of particle size and wavelength and is a proxy for what fraction of radiation is scattered into the forward hemisphere (0 to 90 degrees) verses the backward hemisphere (90 to 180 degrees)

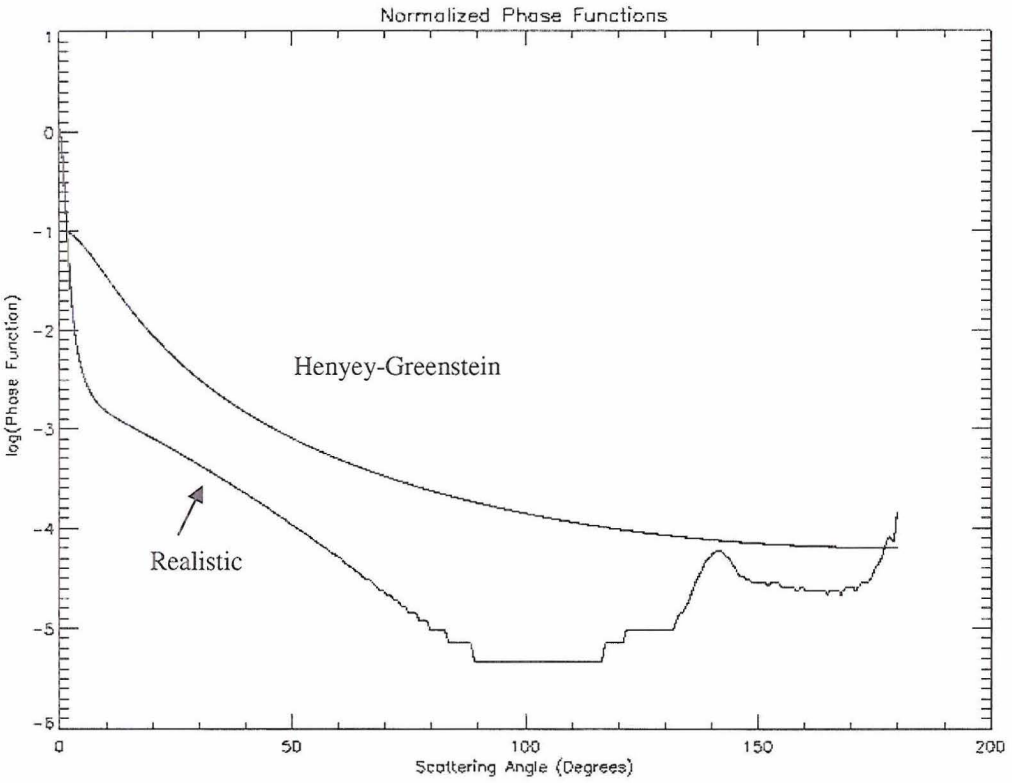

Figure 2.2: A comparison of the realistic scattering phase function, calculated using a Mie scattering code, with the Henyey-Greenstein approximation. Both phase functions are normalized and are for a log-normal particle size distribution with Re = 10 microns and λ = 0.65 microns

Our retrieval utilizes what will be referred to as 'realistic phase functions'. These phase functions are calculated using a sophisticated code that uses the principals of Mie scattering theory for spheres first developed by Gustav Mie in 1908 which produces phase functions that are considered very close to reality. To illustrate the differences in these two methods of phase function calculation, the visible phase functions for an effective radius of 10 microns are compared in Figure (2.2)

The radiative transfer code is developed in such a way that the phase functions are created as a series of Legendre polynomials, which is a standard practice in radiative transfer theory (Gabriel and Christi 2004). The selection of the number of polynomial functions used to recreate the scattering phase function, however, requires the consideration of several factors. The number of polynomials required to adequately represent the phase function's structure is, or course, a function of its complexity. Further, there is a trade off between computational speed and angular resolution realized by the model. A doubling of the number of coefficients doubles the angular resolution of the scattering matrices yet increases computational time by a factor of 8. For our realistic phase functions between 64 and 128 coefficients have been used representing resolutions between 32 and 64 scattering angles with larger values required for larger size parameter cases.

In addition, since the phase functions of interest have extremely strong forward scattering peaks it can be very difficult to recreate them properly with traditional Legendre Polynomial reconstruction. Consequently, the delta-m scaling method is employed (King and Harshvardhan 1986). This approximation takes a large amount of the scattered energy from the forward peak and assumes that it is directly transmitted through the layer instead of subtly scattered. The phase function is then redistributed and the single scatter albedo, optical thickness, and asymmetry parameter are rescaled appropriately.

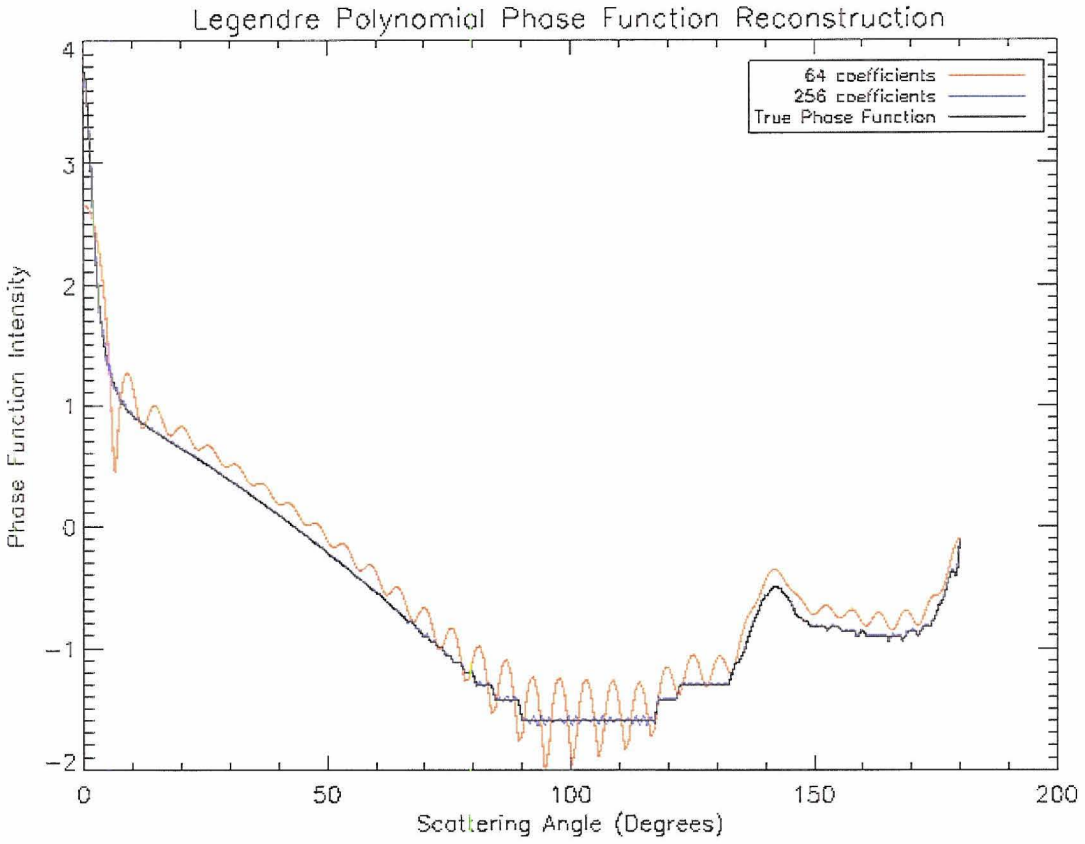

Figure 2.3: Scattering phase function of a log-normal distribution of 10 micron effective radius cloud droplets. Black is the mie-derived phase function, red is the Legendre polynomial recreation of the phase function using 64 coefficients and delta-m scaling, the blue line using 256 coefficients and delta-m scaling.

Examples of the delta-m scaled reconstructions of a 10-micron effective radius particle distribution in the visible are presented in figure 2.3. When too few coefficients are used in the phase function reconstruction, here 64, the resultant representation is very noisy and the amount of energy redistributed by the delta-m scaling method becomes very large, leading to large errors in the resulting radiative transfer solution. However, when sufficient numbers of polynomials are used, here 256, then the delta-m approximation is more subtle and the phase function is almost perfectly captured in the backscatter direction.

The HG phase function is defined by its Legendre coefficients and is given by:

$$\chi^L = (2*L-1)*g^L \quad (2.12)$$

Where, L is the coefficient number and g is the asymmetry parameter.

Scattering phase functions are produced at each wavelength at a series of effective radii with a resolution of 1 micron, r_{eff} = 5μ, 6μ, etc. The Mie theory calculations are performed assuming a log-normal particle size distribution with an effective variance of v_{eff} = .2μ. Two examples of log-normal particle size distributions are shown in Figure 2.4.

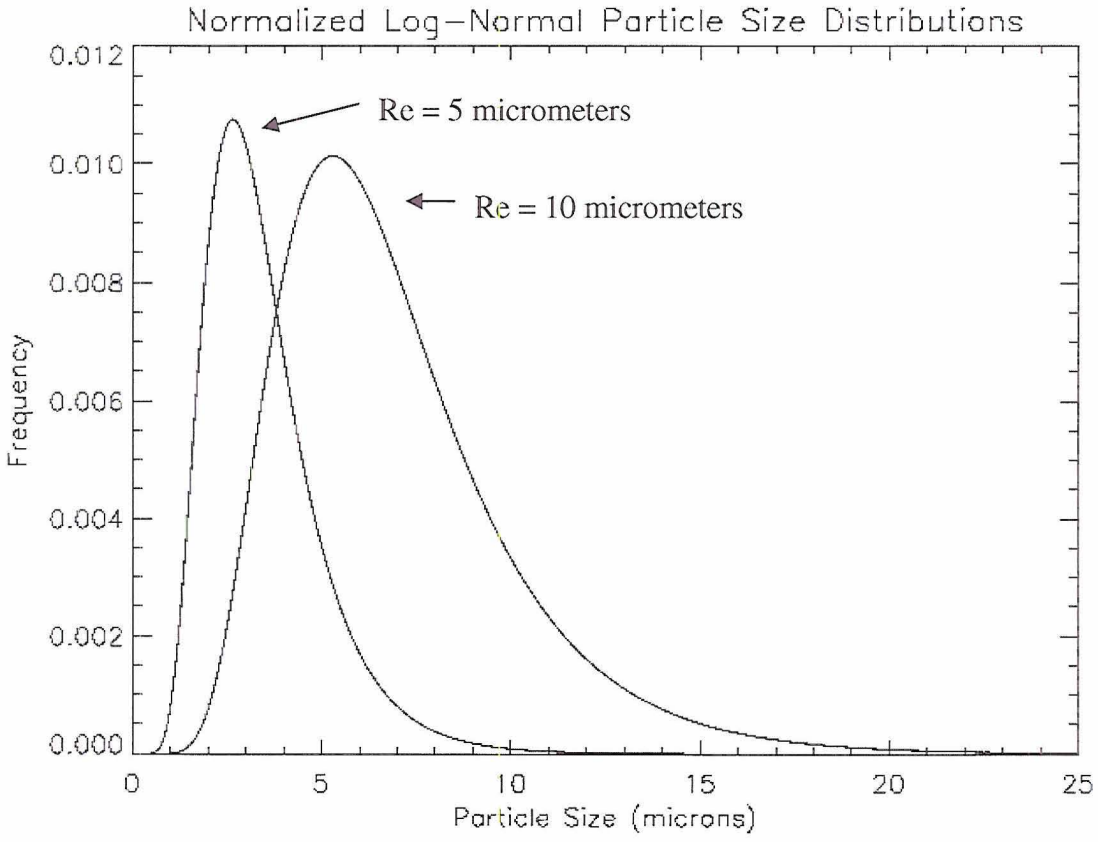

Figure 2.4: Log-normal particle size distributions for effective radii of 5 and 10 microns.

CHAPTER 3: MODIS COMPARISONS

3.1 The MODIS Instrument

MODIS is a radiometer system that measures upwelling solar radiation scattered by the atmosphere as well as emitted infrared radiation in 36 spectral channels that range from 405 nm to 14.3 microns. The channels provide a relatively high spatial resolution ranging from 250 meters in the visible channels to 1 KM in the infrared at nadir. There are two MODIS systems currently in orbit, one on the Terra platform launched in 1999 and another on the Aqua satellite that was launched in 2002. Each system scans from nadir to approximately $\pm 55^{o}$, resulting in a ground swath that is approximately 2000 KM in width.

3.2 The MODIS Cloud Property Retrieval

The MODIS operational retrieval of optical depth and effective radius is essentially an interpolated look up table method (King et al. 1999). Radiative transfer calculations are performed off-line in 4 channels: a non-absorbing visible channel centered near 0.65 microns, 2 shortwave channels near 1.64, 2.13, and an IR channel at 3.7 microns. At each channel, reflectances were pre-calculated for a number of solar and viewing geometries: 42 solar angles, 36 viewing angles, and 33 azimuth angles, as well as 4 optical thicknesses (3,5,8, and ∞) and several cloud particle effective radii. Their model also includes a 1-layer atmosphere above the cloud to account for Raleigh scattering by nitrogen and oxygen molecules as well as water vapor absorption, calculated using a correlated-k distribution (Kratz 1995).

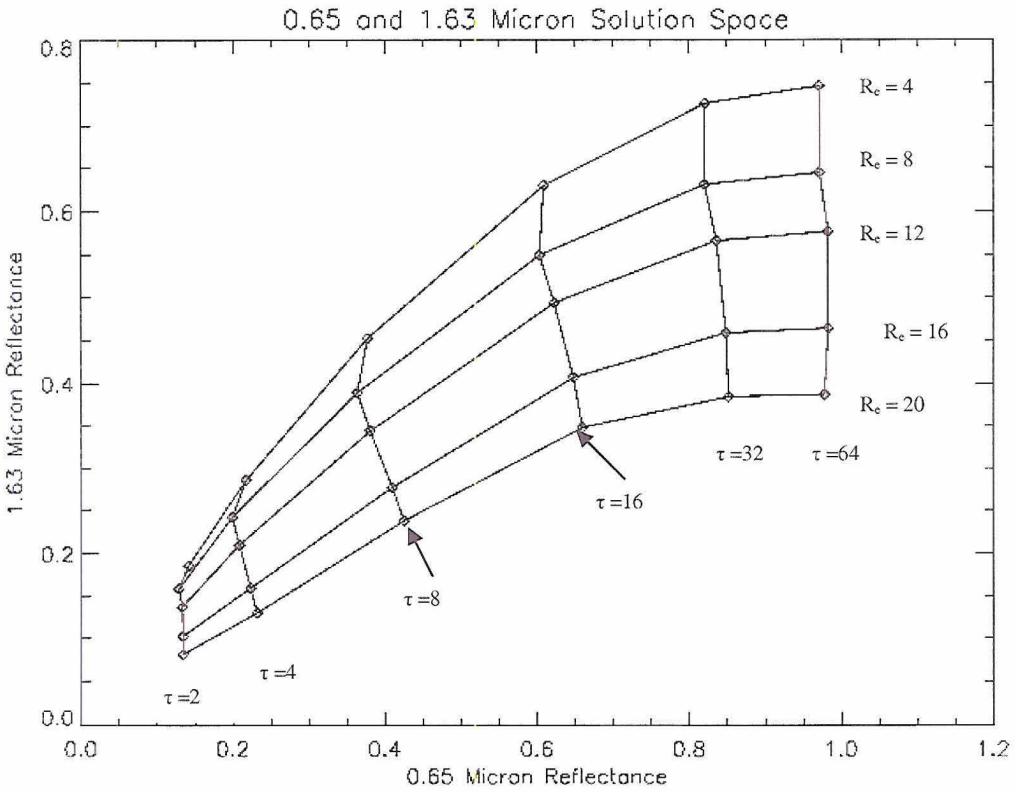

Figure 3.1: Calculations performed by RADIANT for a nadir view with an overhead sun that illustrates the utility of the Nakajima and King retrieval philosophy, which holds that for most typical water clouds simultaneous τ and r_e determination is possible due to the orthogonal nature of the solution space.

Therefore for each daytime field of view (FOV) determined to contain clouds (which is done via a separate IR cloud detection and phase retrieval) the appropriate solar and view angles are selected followed by a chi-squared minimization for each of the 3 wavelength pairs to determine the most likely visible optical depth and effective radius pair. This method is similar to that developed by Twomey and Cocks (1982) and Nakajima and King (1990) and results in one optical thickness estimate but 3 'independent' effective radius estimates. It is important to note that although the three near-IR channels have similar radiative properties, they are not identical. Of interest is the fact that the 3.75 micron channel is characterized by greater absorption by liquid water particles than the 1.63 or 2.13 micron channels. Consequently the latter

channels are more sensitive to cloud particles located deeper in the cloud than the 3.75 micron channel. Differences in retrieved cloud properties using the 1.63 and 2.13 micron channels might be expected to be small since these channels measure only slightly different volumes of cloud whereas the scene when observed by the 3.75-micron channel might be expected to contain significant independent information.

Figure 3.1 illustrates the theoretical basis of the bi-spectral reflectance procedure first conceived by Twomey and Cocks (1982) and applied by Nakajima and King (1990).

Figures 3.2- 3.4 present the 3 MODIS cloud top effective radius retrievals for a nearly overcast, low, water cloud scene observed on 3 June 2001 at 0415Z. The scene, which is roughly 100 Km by 300 Km, was selected for comparison due to the large range of particle sizes observed. It can be seen that, while there is reasonable consistency between the three products, that there are significant differences in the spatial structure, in the number of scenes that produced a converged retrieval, and most strikingly, the median particle size retrieved differs. In this scene the median effective radius retrieved at 3.75 microns is approximately 30% less than that inferred from the 1.63-micron channel.

Figures 3.5-3.7 comprise a similar particle size comparison for an ice cloud case observed during the same orbit on 3 June 2001, the scene is roughly 700 Km square. Here, the 1.63 and 2.13 micron retrievals agree very well, while the 3.75-micron retrieval has trouble converging and tends to estimate larger particle sizes, of order 20%. In ice, 3.75-micron radiation is even more absorptive than in water with an index of refraction of $1.39 + .0067i$ in ice and $1.35 + .0034i$ in water. Therefore it is

inferred that this cirrus cloud scene was characterized by increasing particle size with increasing height within the cloud.

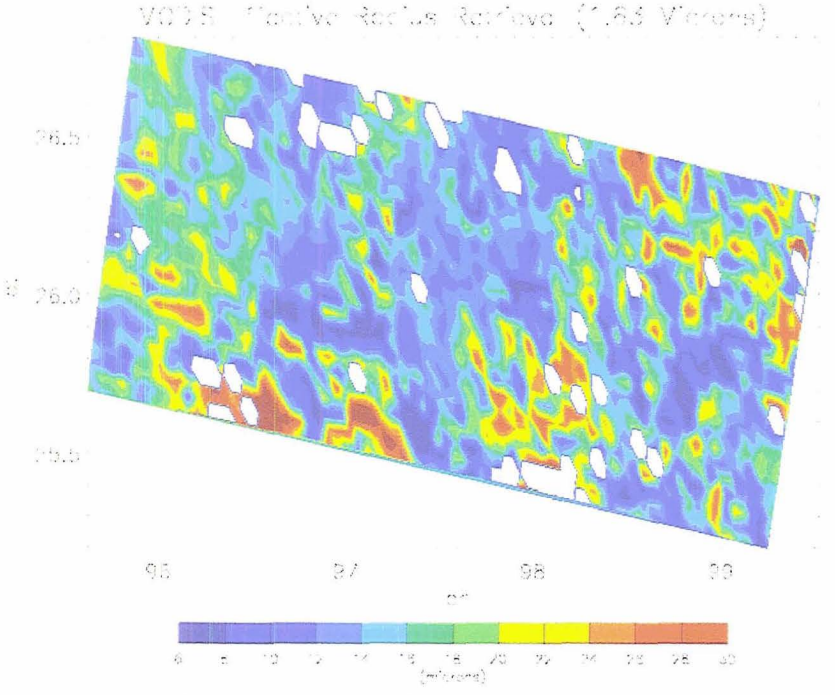

Figure 3.2: MODIS operational effective radius product at 1.63 microns from a water cloud scene from the Gulf of Mexico on 3 June 2001.

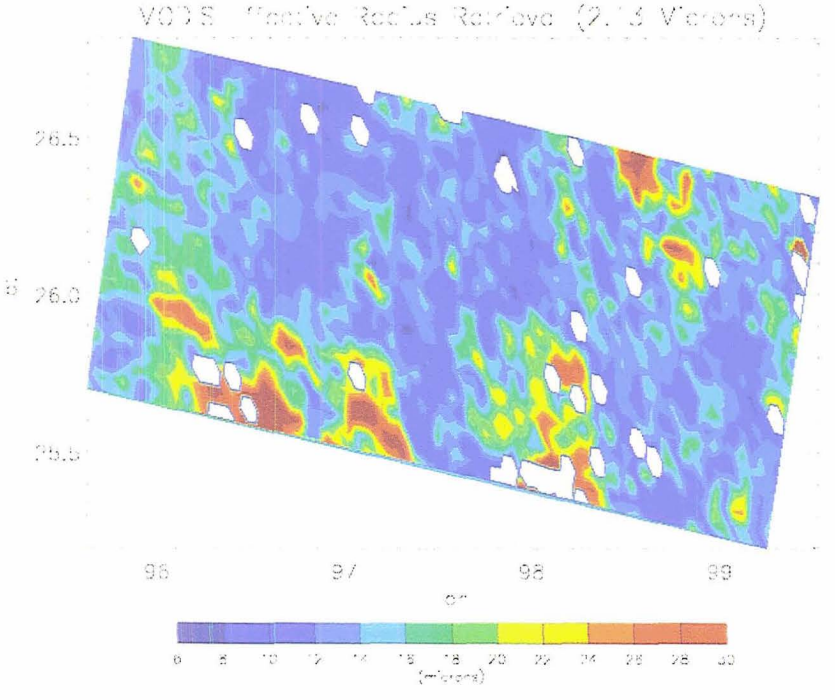

Figure 3.3: Same as 3.2 except at 2.13 microns.

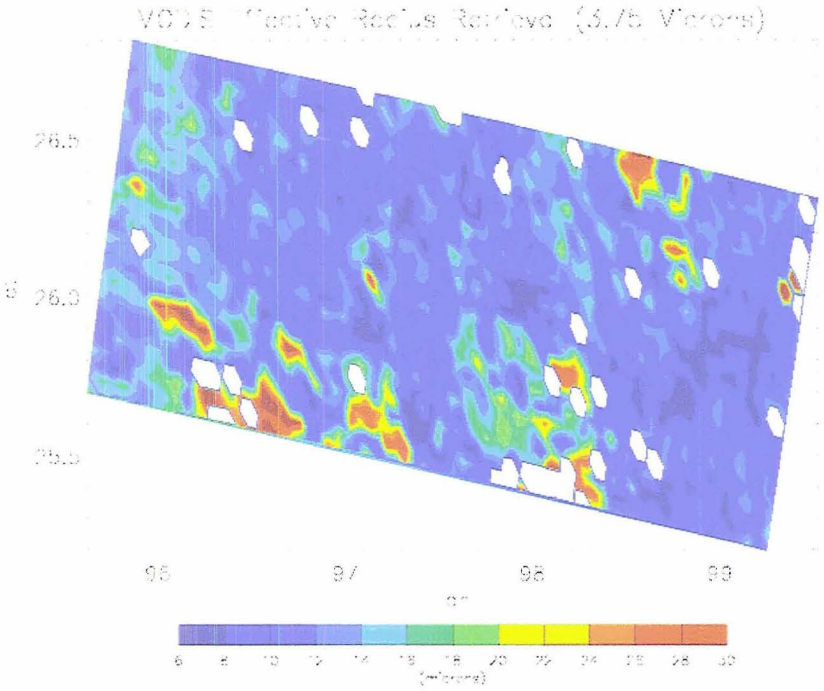

Figure 3.4: Same as 3.2 except at 3.75 microns.

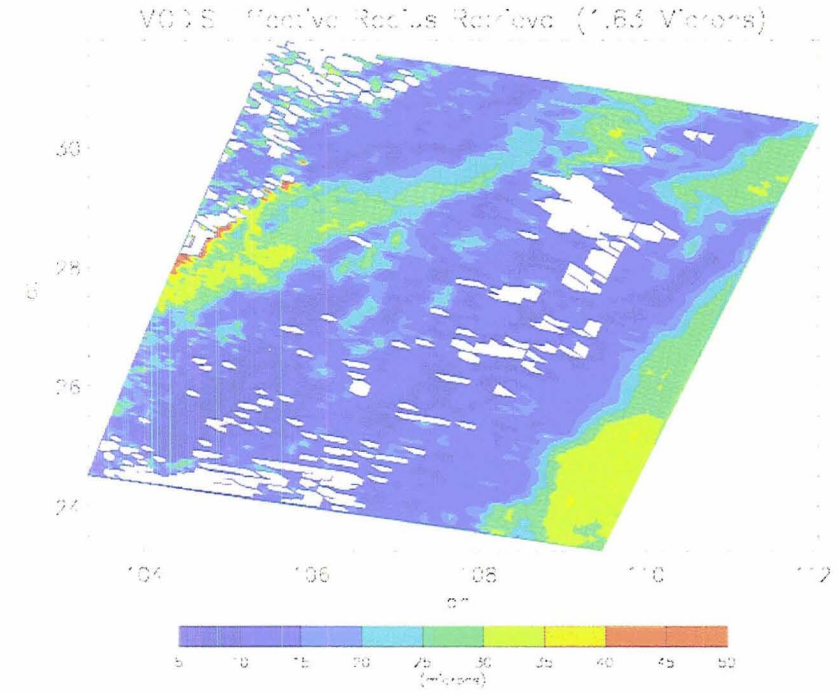

Figure 3.5: MODIS operational effective radius retrieval at 1.63 microns for an ice cloud scene observed 3 June 2001 at 0415Z.

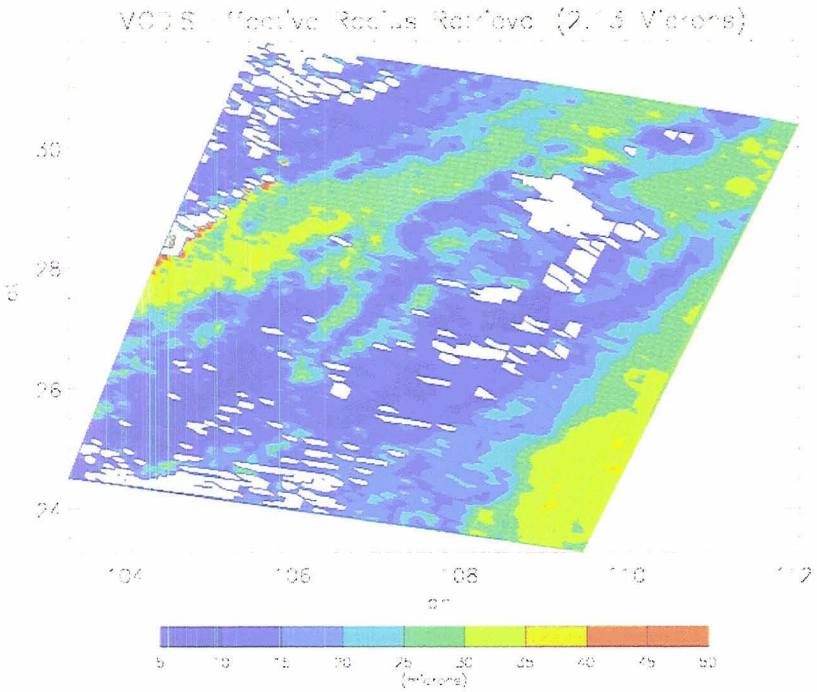

Figure 3.6: Same as 3.5 except at 2.13 microns.

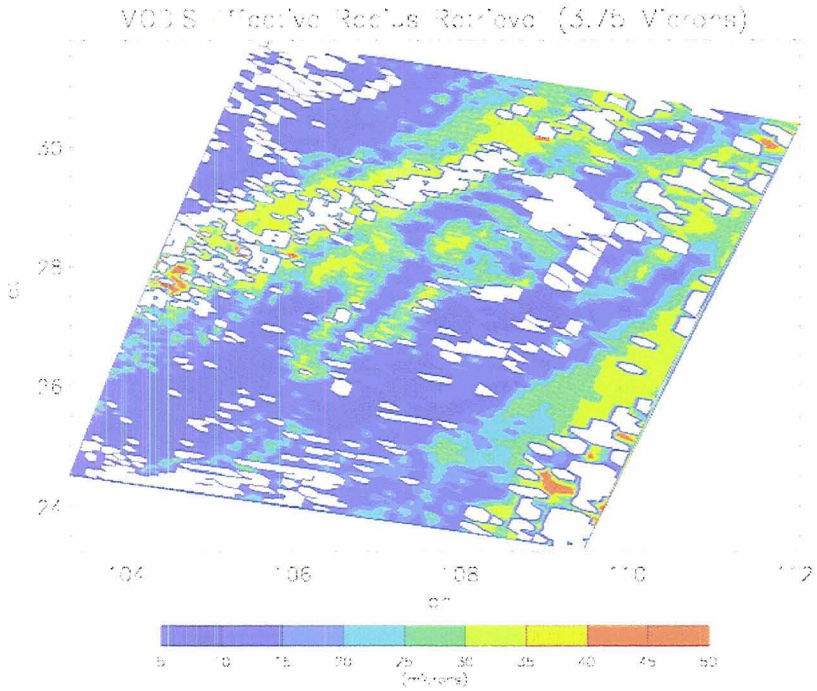

Figure 3.7: Same as 3.5 except at 3.75 microns.

3.3 The Optimal Estimation Retrieval Method

For the cloud retrieval comparisons, 4 MODIS spectral channels were used to retrieve cloud optical depth and cloud top effective radius which were then compared to the MODIS retrievals of these quantities. The visible channel centered at 0.65 microns exhibits near conservative scattering whereas the near-IR channel at 1.6 microns is sensitive to both particle size and cloud optical thickness. The 3.7 micron channel has significant contributions from both solar and terrestrial sources and is also sensitive to both retrieved parameters. Finally, a thermal IR window channel centered near 11 microns is used primarily to place the cloud layer of interest at the appropriate level in the model atmosphere by assuming the cloud to be thermally opaque. Thus the 11 micron brightness temperature, assumed to be the cloud top temperature, is then compared to the NCEP reanalysis derived model atmosphere to determine the most likely cloud height.

Retrievals are only run for cases that are relatively opaque (optical thickness greater than 3 or so) as this partially removes the uncertainties associated with surface reflection and low level water vapor concentrations and in general, provides a more tractable radiative transfer problem. The opacity is estimated off line by considering only cases that have visible reflections over a specified threshold value. Further, for the purpose of comparisons, retrievals are performed only for FOVs which were within 5 degrees of nadir to minimize the three dimensional effects and to remove the azimuthal dependence of the radiative transfer solution. Also, low sun cases, with a solar zenith in excess of 60^{o} were not considered. Finally, the forward model radiances were calculated for phase functions in 2 regimes; a regime in which the

cloud particles are assumed to be spherical water droplets for all scenes with brightness temperatures in excess of 270K and a regime in which cloud particles were assumed to be ice crystals. In the case of the liquid water clouds, phase functions were calculated for particles in 1 micron increments beginning at 1μ and extending to 60μ. For colder clouds, which are more likely composed of ice crystals, phase functions were based on those used in the MODIS ice retrieval. These phase functions used by MODIS consist of a mixture of several different habits of ice crystals characterized by an effective radius spanning 5 to 90 micrometers in 5 μ increments. Although the phase functions for ice crystals provided by MODIS are identical to those used in the MODIS operational retrieval, the water particle phase functions used in the optimal estimation retrieval were calculated using a Mie scattering code as described in section 2.3. Therefore in the water cloud regime the difference in scattering phase functions employed by the two retrievals, while expected to be small, is a potential source of bias.

3.4 Comparisons and Results

The primary purpose of using the MODIS retrieval of τ/r_e in this study was to establish a basis for comparison of the retrieval based on the optimal estimation approach. To this end, only a few carefully selected case study retrievals were performed and compared to the operational MODIS retrieval. It was not expected that the optimal estimation results would exactly map to the MODIS solution since each retrieval uses different sets of assumptions regarding the state of the atmosphere and radiative transfer solutions. Consequently, both retrieval methods have their own

systematic and random errors. Principal amongst these is the fact that the operational MODIS retrieval algorithm uses 2 channels with no error assumptions placed on the observations or the forward model, while the optimal estimation retrieval uses 3 channels and accounts for errors in the observations and in the forward model.

In order to isolate retrieved microphysical discrepancies due to the radiative transfer implementation; the optimal estimation method was run in its full 3-channel mode as well as a 2 channel mode that assumes zero error in the measurements and radiative transfer solution in an attempt to match the operational MODIS inverse procedure. The 2 channel simulator mode not only eliminates biases arising from differences in the retrieval methodologies and their underlying assumptions, but further, in the ice cloud case, eliminates biases associated with the scattering phase functions.

3.4.1 Ice Cloud Comparisons

The ice case presented is a subset of a cirrostratus cloud field observed by MODIS on 5 Nov 2002 centered near 15^{o} south latitude and 165^{o} west longitude in the south central Pacific Ocean. The retrieved area is approximately 50 Km square with cloud heights between 8 and 10 Km. The solar zenith angle was approximately 15^{o} and the view angle was between $1\text{-}3^{o}$.

For this case, the optimal estimation retrieval was run in the MODIS simulator mode using the 0.65-μ visible channel as well as at 1.63 μ. Figures 3.8 and 3.9 compare the effective radius and optical depth retrieval between the MODIS simulator and the operational MODIS retrieval. The effective radius results in figure

3.8, show good agreement between the optimal estimation and both the MODIS 1.63 and 2.13 micron retrievals, with very little bias, however with admittedly large scatter. The optical thickness retrievals are for most of the scene in good agreement with the operational MODIS solution, exhibiting in general slightly smaller optical thicknesses except for the anomalous behavior in the in the range $6 < \tau < 8$. This behavior is likely due to the cloud scenes being classified by MODIS and the optimal estimation retrieval in a different way, perhaps with respect to solar angle, view geometry, or cloud height or phase determination. Notwithstanding these few cases, this cloud scene seems to show good agreement, at least within the estimated retrieval uncertainties, between the two retrieval methods, especially for effective particle size.

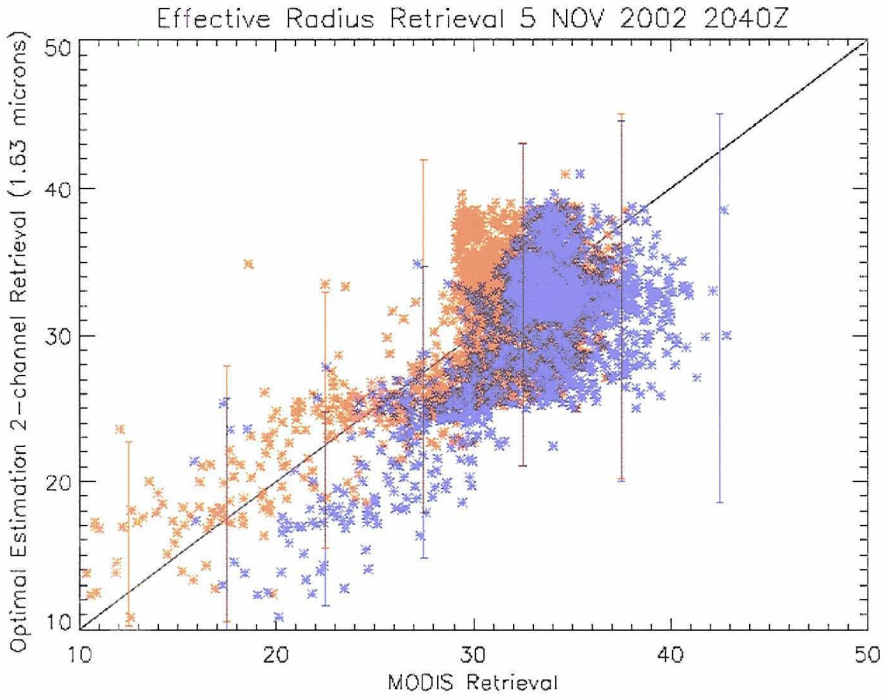

Figure 3.8: Comparison of the MODIS operational retrieval Blue – 1.63 microns, Red – 2.13 microns, against the 2-channel optimal estimation MODIS simulator retrieval for an ice cloud case 5 Nov 2002 in the South Pacific Ocean. Superimposed at 5 micron intervals , vertical bars represent median errors centered at median optimal estimation retrieved values.

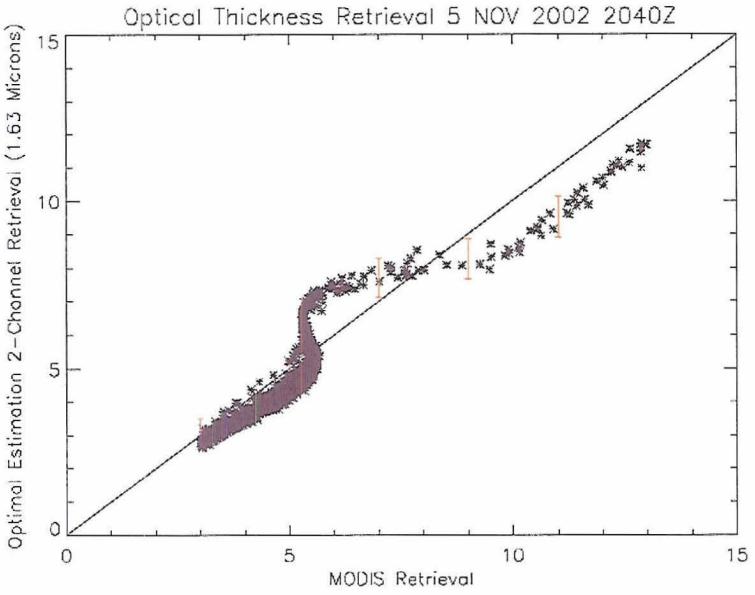

Figure 3.9: Comparison of MODIS operational optical depth retrieval with MODIS simulator 2-channel retrieval (1.63 micron). Ice cloud scene 5 Nov 2002, South Pacific Ocean. Superimposed at 5 micron intervals , vertical bars represent median errors centered at median optimal estimation retrieved values.

Figure 3.10, presents a comparison of ice cloud effective radius retrievals between the operational MODIS retrieval and the full 3-channel optimal estimation retrieval. Here the optimal estimation retrieval has been shifted to somewhat smaller values for r_e and now exhibits a negative bias relative to the operational MODIS solution, although still within the estimated range of uncertainty. The difference can be explained by the following observations: since ice exhibits extremely strong absorption in the 3.75 micron channel, the resulting weighting function of this band peaks nearer the cloud top than either the 1.63 or 2.13 micron channels. Since cloud particle sizes typically decrease with increasing height in ice clouds, the 3.75 μ radiances will act to "pull" the results toward smaller particle sizes. Second, the introduction of error statistics via the error covariance matrices will result in an independent result via the implementation of the optimal estimation mathematical

framework. It should be noted that due to the large errors associated with the ice particle size retrieval, it cannot be said with any certainty that the optimal estimation solution is statistically or physically distinct from the MODIS operational solution in either the 2-channel or 3-channel formulation. What can be said with certainty is, due to the identical method employed, for this scene, the introduction of the 3.75-micron spectral information reduces the estimated cloud top particle size. The role of the error covariances in influencing the optimal estimation solution is discussed further in section 3.5.

The optical depth retrieval, not shown, exhibited a behavior similar to the 2-channel retrieval.

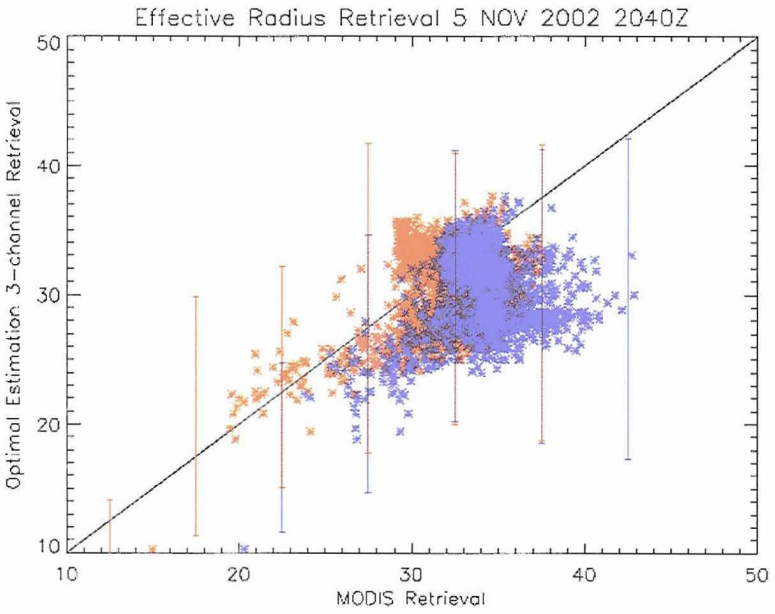

Figure 3.10: Comparison of operational MODIS effective radius retrieval, Blue – 1.63 microns, Red- 2.13 microns, with the 3-channel optimal estimation retrieval. Vertical bars indicate median errors.

3.4.2 Water Cloud Comparisons

The first water cloud case presented is a subset of a stratiform cloud field observed by MODIS on 7 July 2001 at 2030Z centered near 38 North latitude and 141 West longitude in the northeastern Pacific Ocean, the cloud scene area being approximately 200 Km by 200 Km. The solar zenith angle was approximately 32° over that region at that time and the viewing angle was near nadir.

Figure 3.11 presents a comparison of the MODIS operational optical thickness retrieval with that calculated from the optimal estimation retrieval. For this case very good agreement is found between the two approaches, with the optimal estimation retrieval showing a slight positive bias of less than 10% in the mean with a small variance. In contrast, a comparison of the retrieved effective radii for this case, presented in figure 3.12, shows that the operational MODIS particle size retrievals are up to 100% larger than those inferred using the optimal estimation approach, but that

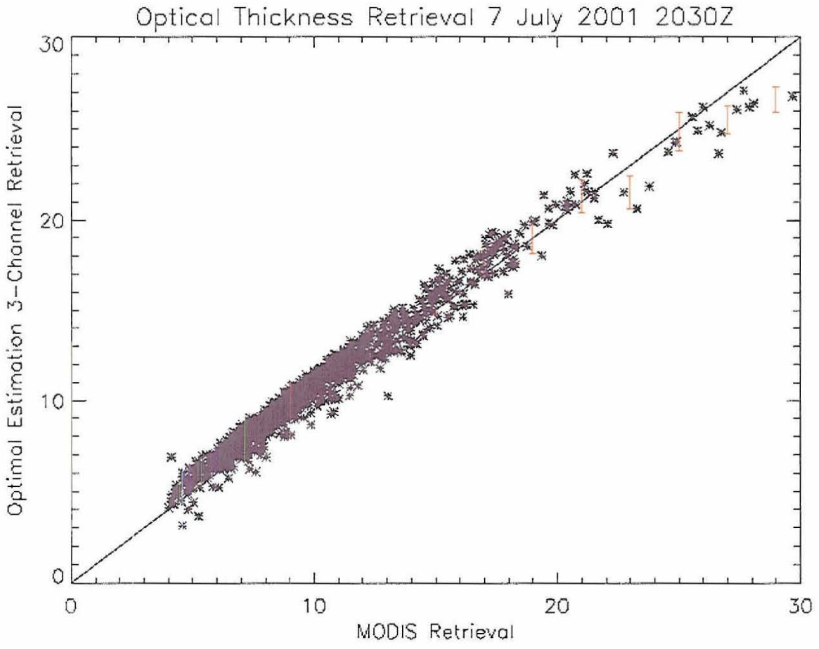

Figure 3.11: Comparison of retrieved optical depths between the 3-channel optimal estimation retrieval with the operational MODIS retrieval. Shows a slight positive bias in the optimal estimation solution. Vertical bars indicate typical errors.

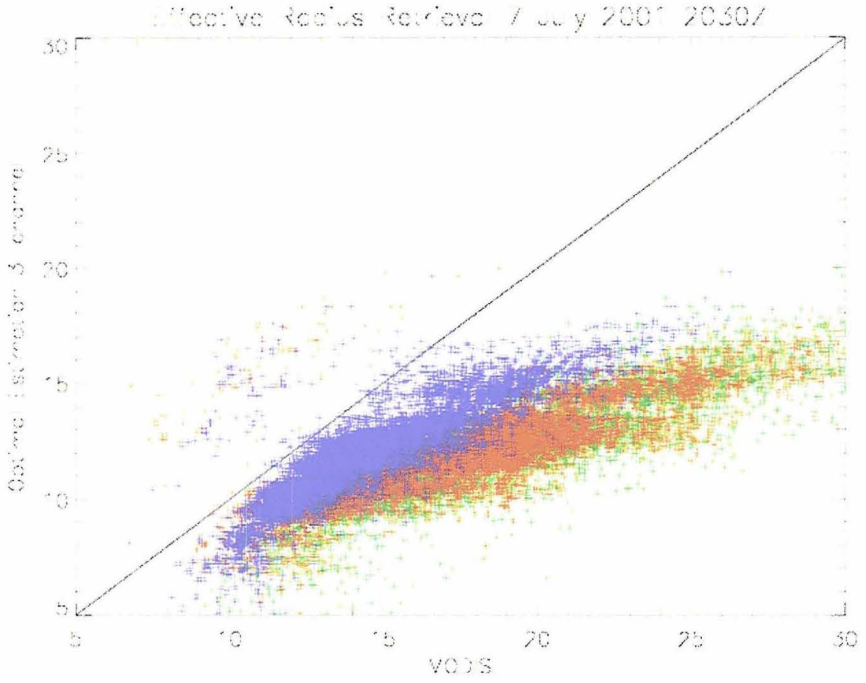

Figure 3.12: Comparison of the effective radius between the 3-channel optimal estimation retrieval and the 3 operational MODIS retrievals. Red – 1.63 microns, Green-2.13 microns, Blue – 3.75 microns 7 July 2001

these operational estimates vary among themselves by almost a factor of 2. Table 3.1 summarizes the median biases between the 3-channel optimal estimation retrieval and other retrievals examined in this section.

Figures 3.13 and 3.14 show the spatial distribution of the retrieved effective radius for the scene using the optimal estimation retrieval as well as the percentage difference between the MODIS 1.63 micron retrieval and the 3-channel optimal estimation retrieval. It is clear that despite the fact that the bias between these two solutions is large, it is relatively uniform over the cloud scene, suggesting that the bias is systematic. A portion of this bias is due to the introduction of information at 3.7 μ as well as the independent mathematical framework as discussed above. An examination of theoretical weighting functions of particle size sensitivity in water clouds for the MODIS spectral channels was performed by Platnick (2000).

Retrieval	Median Value	Bias Relative to OE 3-channel (%)
OE 3 Chan Re	11.05	N/A
OE 2 Chan Re(3.75)	10.43	-5.7
OE 2 Chan Re(1.63)	13.64	+23.5
MODIS Re(1.63)	15.94	+44.2
MODIS Re(2.13)	15.15	+37.1
MODIS Re(3.75)	13.03	+17.9
OE 3 Chan Tau	9.105	N/A
OE 2 Chan Tau(1.63)	10.02	+10.0
OE 2 Chan Tau(3.75)	9.43	+3.5
MODIS Tau	8.36	-8.2

Table 3.1: Comparison of median results of optical depth and effective radius from other retrieval methodology with the 3-channel optimal estimation solution

These factors were shown to introduce negative optimal estimation differences of 5 to 20% percent in the effective radius retrieval, depending on channel. The water cloud retrievals, by contrast, have negative effective radius prejudice of 20 to 40%. The primary difference between the ice and water cloud cases is that the water clouds

are located much nearer the surface and therefore are observed through a much greater depth of atmosphere, amplifying the effect of the models' atmospheric assumptions. This factor appears to be the genesis of additional 15 to 25% negative differences in the effective radius retrievals, as well as small but significant positive biases in the optical thickness retrieval. The biases observed in optical thickness and particle size are physically consistent with each other implying that the OE forward model radiative solution is producing slightly "darker" reflectances than the MODIS operational radiative transfer solver. That is, the optimal estimation solution is compelled to move towards "brighter" retrieval solutions in order to minimize its cost function. The result is a retrieved atmospheric state characterized by smaller particle sizes and larger optical depths. Without knowing the details of implementation of the MODIS radiative transfer solver it is impossible to deduce which solution is more correct, but from the evidence, it appears that the use of independent scattering phase functions, and more significantly, atmospheric correction methods, characterize the dominate sources of disagreement.

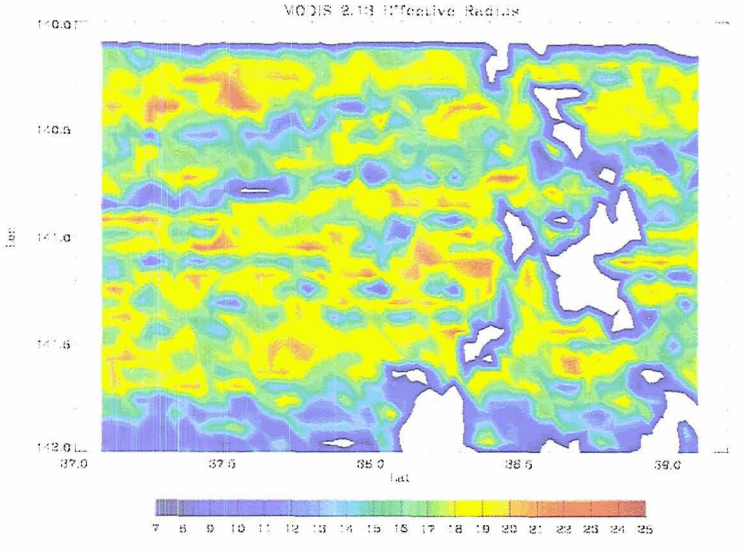

Figure 3.13: Effective radius retrieval of a stratus cloud scene, 7 July 2001 over the NE Pacific Ocean. This scene is 200 Km square, and is located near 38° N, 141° W.

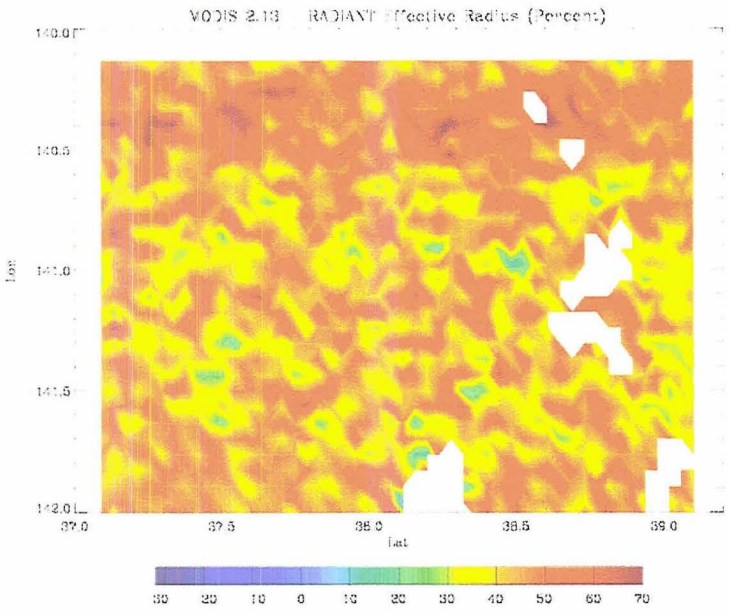

Figure 3.14: Pecentage difference between the operation MODIS 1.63 micron retrieval and the 3-channel optimal estimation retrievals effective radius. This is the same cloud scene as in 3.3

Figure 3.15 shows the MODIS 1.63 micron retrieval of effective radius plotted against the optimal estimation 3-channel retrieval for a subset of the stratus cloud scene discussed above on 7 July 2001 . Again there are significant differences between the two retrievals, with the operational MODIS solution approximately 45% larger than that of the optimal estimation method in the mean. However, when the MODIS retrieval is compared with the 2-channel MODIS simulator retrieval, in figure 3.16, it is clear the difference with the MODIS operational retrieval is reduced somewhat to about 20% in the mean. Somewhat different results were found when the MODIS 3.75 micron wavelength retrieval was used. When compared to the full 3-channel retrieval, figure 3.17, the effective radius values inferred by MODIS show an

overestimation of approximately 20% relative to the OE approach. In addition, when the more direct MODIS simulator OE method is compared to the operational MODIS product, figure 3.18, very little reduction is bias is observed, but the two solutions appear more tightly correlated. This observation may, in part, be understood by noting that the phase function effects at 3.75 μ would be reduced relative to the 1.63 or 2.13 μ channels since there is less scattering by water or ice in this spectral region. In this channel, the reflectance is highly sensitive to the location of a cloud as well as the temperature and water vapor profiles above the cloud. Consequently, it appears that the primary source of model brightness disagreement in the 3.75-μ case is due not to the scattering phase function but to the details of the atmospheric correction employed by the two retrieval implementations.

Thus far, little has been said about optical thickness retrieval comparisons. These retrievals showed very good consistency, being highly correlated with the MODIS solution in all cases, showing a smaller than 10% departure from the MODIS solution that shifted slightly with the effective radius biases for each case. In general, larger optical thickness biases were associated with larger effective radius biases.

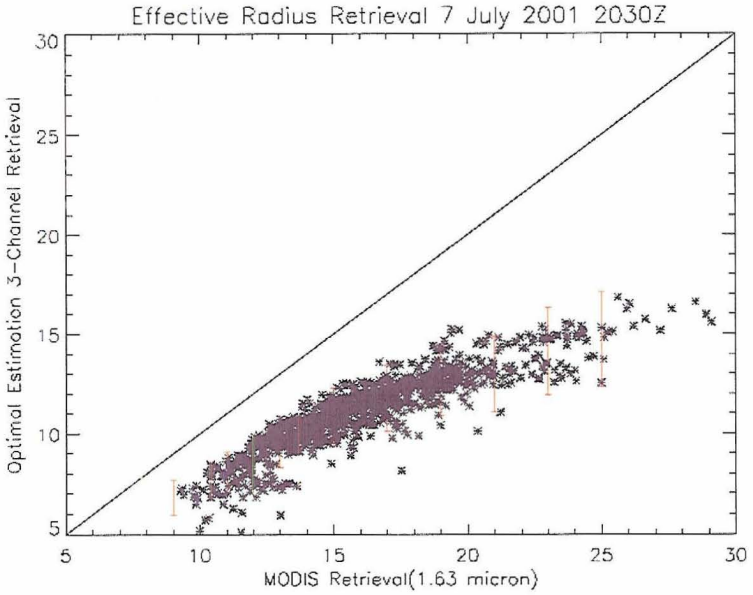

Figure 3.15: Comparison of effective radius between 3-channel optimal estimation retrieval with operational MODIS 1.63 micron product, 7 July 2001. Vertical bars indicate median errors.

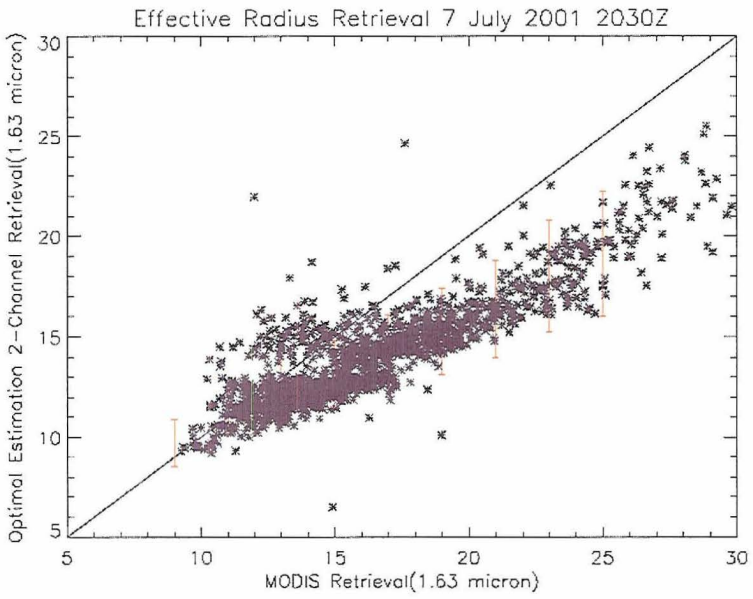

Figure 3.16: Comparison of effective radius retrieval between 2-channel MODIS simulator retrieval (1.63 microns) and operational MODIS 1.63 micron retrieval 7 July 2001. Vertical bars indicate median errors.

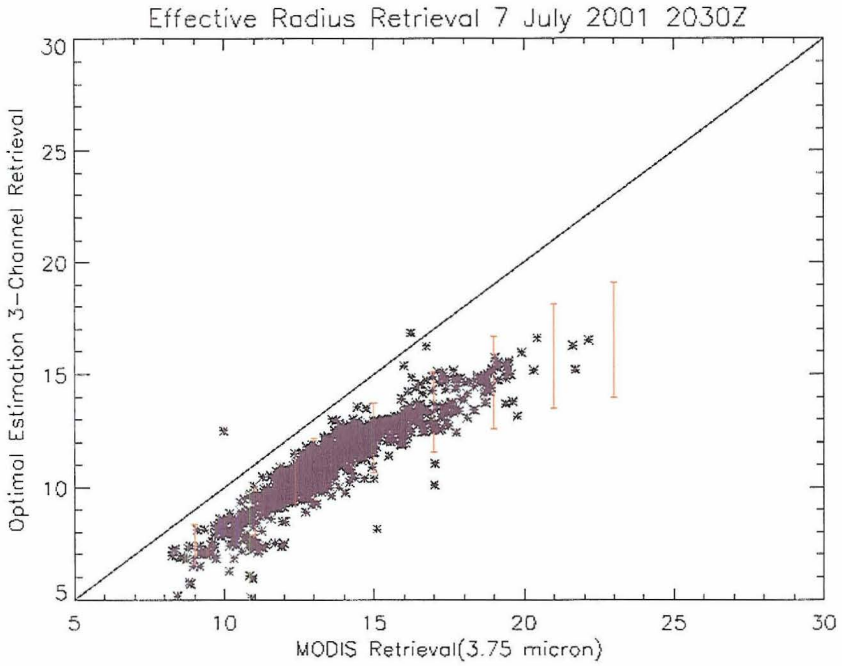

Figure 3.17: Comparison of effective radius between 3-channel optimal estimation retrieval with operational MODIS 3.75 micron product, 7 July 2001. Vertical bars indicate median error.

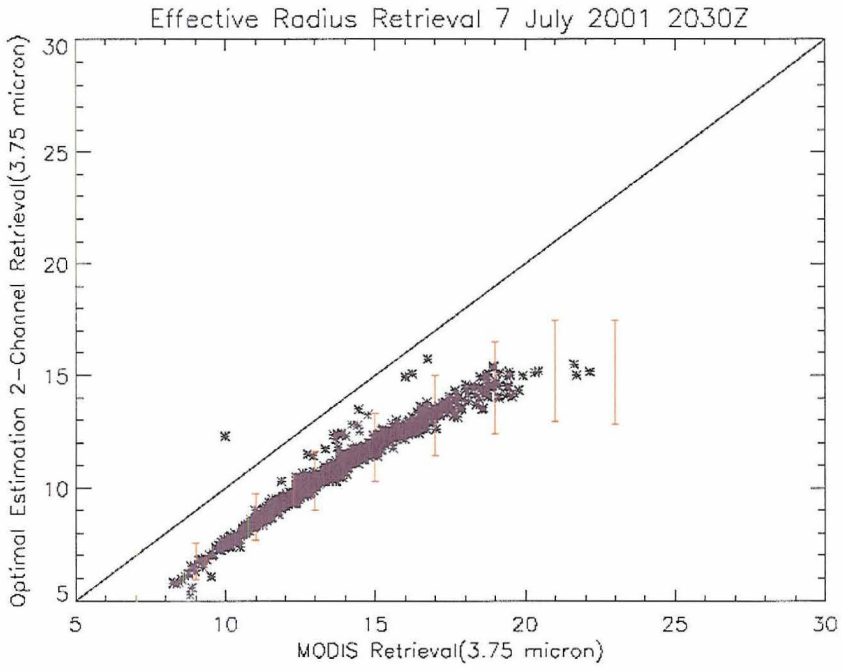

Figure 3.18: Comparison of effective radius retrieval between 2-channel MODIS simulator retrieval (3.75 microns) and operational MODIS 3.75 micron retrieval 7 July 2001. Vertical bars indicate median errors.

It is important to note that the observed biases in the effective radius as a function of channel in the above cases are not consistent for all scenes or viewing geometries. Data from another case taken on 4 July 2001 at 1955Z located in the Pacific Ocean centered near 52° N and 131° W was characterized by broken water cloud. However, only scenes with cloud fractions greater than 90%, as determined by the MODIS product, were compared. For this case, the solar zenith angle was about 16^{o} with a viewing angle nearly nadir. Figure 3.19 presents a comparison of the 3-channel optimal estimation effective radius, with the 3 operational MODIS products. The results show very little difference in the retrieved MODIS effective radius between the three channels, implying that the cloud particle sizes are relatively consistent throughout the upper several hundred meters of these clouds. As a result, the effect of introducing the third channel had little effect on the solution and the observed biases were almost exclusively due to differences in the radiances caused by differences in the models' atmospheric assumptions or by differences in the temperature and moisture profiles. Further, even after isolating only model induced effects as described in the previous analysis, the effective radius biases in this case here are only of order 10%. The comparison of optical thickness retrievals in figure 3.20, similarly shows good agreement with very small bias. It seems that though large biases between the model solutions can occur, as seen in the 7 July case, that this may not be typical, as the results from the 4 July case, using identical procedures, produce much more consistent results.

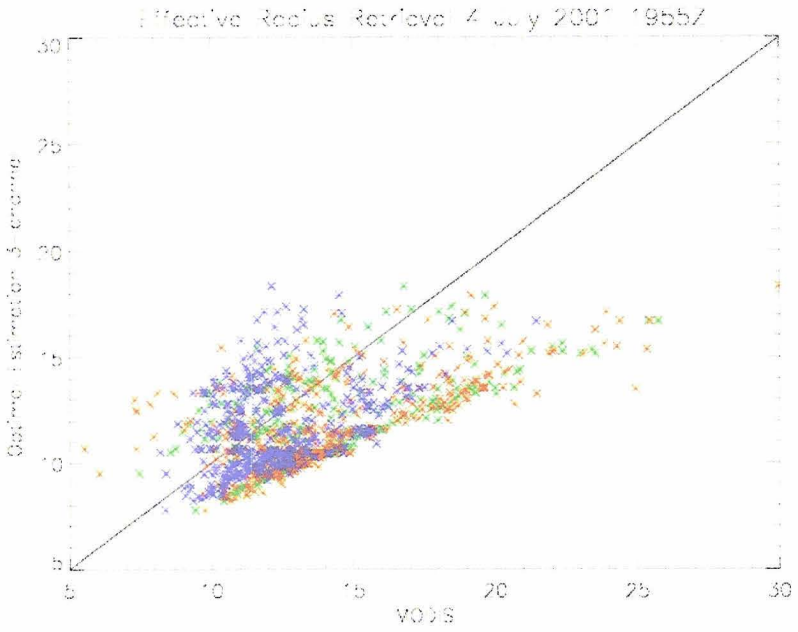

Figure 3.19: Comparison of the effective radius between the 3-channel optimal estimation retrieval and the 3 operational MODIS retrievals. Red – 1.63 microns, Green-2.13 microns, Blue – 3.75 microns

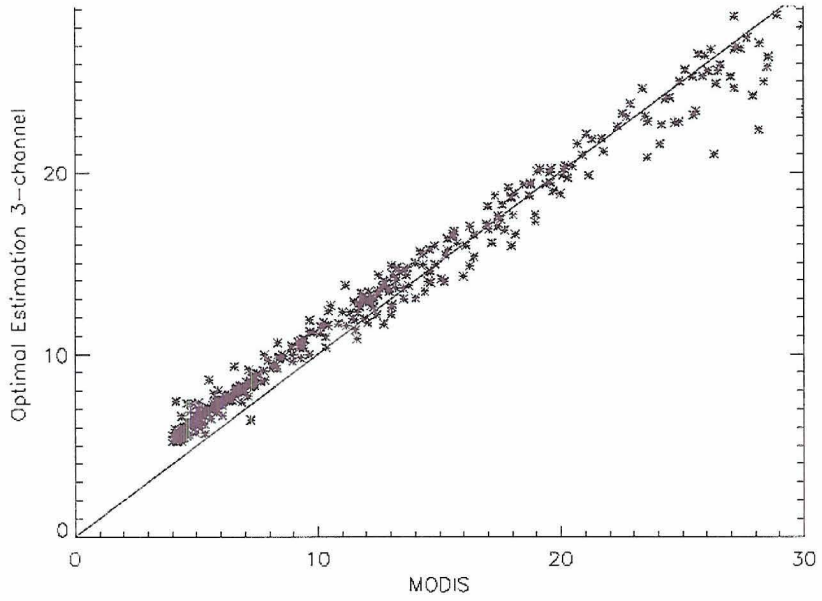

Figure 3.20: Comparison of retrieved optical depths between the 3-channel optimal estimation retrieval with the operational MODIS retrieval. Shows a slight positive bias in the optimal estimation solution.

3.5 Summary and Discussion

- The retrieved effective radii of the operational MODIS product and the optimal estimation result exhibit a significant bias, the magnitude of which is strongly scene dependant.
- The operational MODIS product, itself, produces 3 "independent" particle size estimates that contain significant internal inconsistency.
- For water clouds, the MODIS operational product overestimates the OE effective radius by 10-45% and underestimates the optical thickness by as much as 10%, depending on scene.
- Comparisons using a 2-channel "MODIS simulator" retrieval reduced the magnitude of the bias somewhat, by eliminating differences associated with inverse procedures and introducing the 3.75-μ channel, thought to contain independent physical information.
- Agreement is found to be significantly better for ice cloud scenes.
- The source of disagreement, especially for warm cloud scenes, is not fully known, due to incomplete knowledge of the MODIS radiative transfer procedure, but is likely a function of the assumed state of the atmosphere (e.g. temperature and moisture profiles and gaseous correction procedures).

It is natural to assume that the more fully developed 3-channel optimal estimation approach would produce not only different, but also better and more accurate results. However, it is important to realize that only the introduction of appropriate and accurate error characterizations would act to reduce the overall error in the final

analysis: in a sense there is no free lunch. In the retrievals presented here, care has been taken to accurately assess the errors typical of the forward model and of the observing system for plane parallel clouds (section 2.1), and in the selection of cloud scenes and viewing geometries that act to minimize the influence of 3 dimensional effects on the observed radiance field. With this in mind, it is argued that the 3-channel operational retrieval presented above is superior to the 2-channel MODIS retrieval, which does not provide retrieval uncertainty estimates and relies on less spectral information, for these carefully selected cloud scenes. However, it is important to realize that blindly applying error covariances to a scene for which they do not necessarily apply can lead to degradation in the optimal estimation method solution accuracy as opposed to an improvement as well as inaccurate error characterization.

CHAPTER 4: VIRS CLOUD RETRIEVALS

4.1 Instrument Description

The Visible and Infrared Scanner (VIRS) is a 5-channel passive space-borne radiometer on the Tropical Rainfall Measurement Mission (TRMM) satellite that was launched in 1997. Its spectral channels approximately overlap with five MODIS wavelengths and are centered near 0.65, 1.6, 3.7, 11.0, and 12.0 microns. The instrument scans from nadir to $\pm 45^{\circ}$ covering a swath approximately 720KM in width. The VIRS has a nominal resolution at nadir of approximately 2.2 KM. In addition, other instruments on the TRMM platform, the TRMM Microwave Imager (TMI) and Precipitation Radar (PR) will facilitate the determination of precipitating cloud scenes.

The TMI is a 5-channel, passive, microwave sensor that is used to retrieve surface wind speed, column water vapor amounts, sea surface temperatures, and rainfall rates (Kumerrow 1998). The 5 microwave frequencies are centered near 10.7, 19.4, 21.3, 37, and 85.5 GHz. The instrument scans in a cone of constant 53° incidence, with a rather large footprint of approximately 16 Km. Due to the smaller microwave emissivities of the ocean surface compared to land, passive microwave retrievals are more tractable over ocean surfaces where greater contrast is found between the radiometrically "colder" ocean surface and the "warmer" cloud particles.

The PR is a radar system operating at a frequency centered near 13.8 GHz. At this frequency, the radar is sensitive to precipitation-sized particles, but suffers from attenuation at very high rain rates. The PR has a scan width of 220 Km with a horizontal resolution of 4.3 Km at nadir. The system provides 3-D rain rate distributions, with a vertical resolution of 250 meters; to a height of 20 Km. Rainfall rates as small as 0.7 mm/hr can be detected with confidence.

The cloud top particle size and cloud optical thickness retrieval designed for the VIRS instrument that is central to this work is descried in detail in Chapter 2.

4.2 Retrieval Procedure

VIRS cloud property retrievals were performed for a large number of warm cloud scenes during January 1999 as well as for a variety of warm and ice clouds during July 1999. Retrievals were limited to nadir pixels, oceanic scenes, and for clouds with an optical depth in excess of roughly 3. Only relatively opaque clouds were examined to reduce the role of surface reflection as well as to mitigate errors due to incorrect vertical placement of the clouds within the model atmosphere. Oceanic scenes were selected to further reduce the errors associated with surface emission and reflection. Finally, retrievals were limited to VIRS' pixels closest to nadir since this viewing geometry is likely to minimize the role of the 3-D structure of clouds in determining the radiance field. Furthermore, the computational expense of the forward model limits the total number of scenes that could be examined. Thus, global statistics and spatial patterns are derived from a sub-set of the VIRS swath. Also, data used from the nadir view angle provides a more straightforward comparison with the TMI and

PR. Collocations with these instruments provide a unique opportunity to determine the statistics of cloud optical depth and cloud top particle size in precipitating as well as non-precipitating clouds.

Roughly 1 million warm cloud cases, as well as 400,000 ice cloud cases were observed for the two month period resulting in approximately 900,000 converged retrievals. The fact that roughly 30 percent of cases that were identified by the cloud mask were inappropriate for retrieval is not entirely surprising, since there are several factors that can lead to a bad retrieval. First, our cloud mask is quite rudimentary, using only a visible reflectance threshold. This can often lead to the identification of badly broken cloud scenes. Since these scenes are at odds with our forward model's plane parallel assumption, we have little chance of properly simulating the observed radiance field. Further, our model atmospheres are, due to the resolution of the NCEP data set, discretized in 2.5-degree lat/lon boxes and at 6-hour intervals and therefore may not be representative of the actual scene. Also, our determination of cloud phase is based on the 11-μ brightness temperature, with a threshold value of 270K. Though it is realized that this simple method will result in a significant number of incorrect phase determinations, due to the existence of supercooled water clouds, these errors are not expected to influence the results. Since the scattering phase functions for water and ice particles are quite different, incorrect phase determination would likely result in a non-convergent solution.

As a note, ice particle sizes in this chapter are expressed in terms of effective diameter, in accordance with the units associated with the supplied MODIS ice scattering phase functions. Effective diameter is defined as:

$$D_e = \int LD(L)^2 n(L)\, dL / \int LD(L)\, n(L)\, dL \quad (4.1)$$

where D is the ice particle width, which is a function of particle maximum dimension (L), and n(L), the particle size distribution. It should be noted that D is also a function of crystal habit, which represents an implied summation within the above equation (King et al. 1999).

4.3 Comparisons With ISCCP

The International Satellite Cloud Climatology Project (ISCCP) uses a variety of satellite data to determine the statistics of cloud fraction and other cloud characteristics around the globe. In all, nearly 130 characteristics are determined of which cloud top temperature and pressure, cloud optical thickness, cloud types, cloud fraction, and cloud phase are relevant to this study. Cloud classification is performed using cloud top pressure and optical thickness as features that place clouds into 9 general categories as seen in figure 4.1 (Rossow et al. 1996).

Since the optimal estimation cloud retrieval returns cloud optical thickness as well as cloud top height, which can be easily converted to cloud top pressure, it was natural to make a direct comparison between the VIRS retrievals the ISCCP climatology. For the month of July 1999, all clouds (ice and water) were compared in the entire TRMM region (global oceans between 35° S to 35° N latitude) as well as for the Tropical West Pacific (TWP) region (130° E to 170° W longitude and 30° N to 30° S latitude). Since the optimal estimation retrieval presented does not retrieve clouds with optical thicknesses less than about 3.0, categories associated with the optically thinner clouds (e.g. cirrus) are not considered.

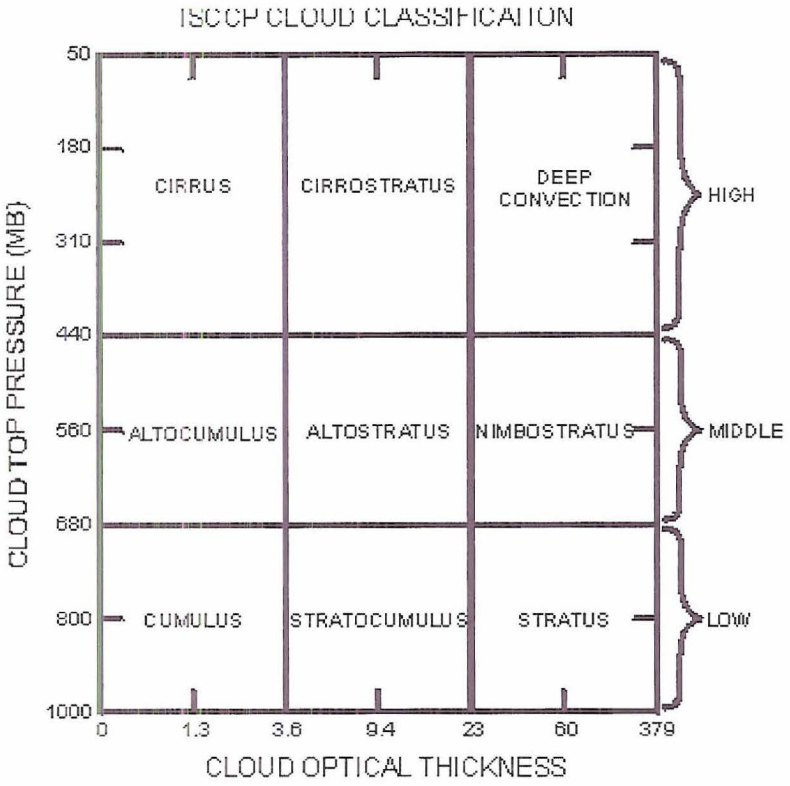

Figure 4.1: Schematic of the ISCCP cloud type determination. 9 cloud types are distinguished as a function of optical thickness and cloud top pressure.

CIRROSTRATUS .156 .185	DEEP CONVECTION .078 .054
ALTOSTRATUS .184 .157	NIMBOSTRATUS .039 .019
STRATOCUMULUS .505 .545	STRATUS .035 .039

Table 4.1: Relative cloud frequency by ISCCP cloud type for the entire TRMM region comparing the ISCCP data in red and the VIRS retrievals in blue.

The relative frequency of the 6 optically thick categories in the TRMM region are compared in table 4.1. In general, there is good agreement between the two distributions, considering that although the comparisons are made over the same

regions for the same month, the optimal estimation retrieval uses only a small subset of the cloud scenes present in the ISCCP climatology. It is clear that the

CIRROSTRATUS .370 .506	DEEP CONVECTION .204 .128
ALTOSTRATUS .164 .164	NIMBOSTRATUS .028 .028
STRATOCUMULUS .217 .157	STRATUS .014 .018

Table 4.2: Relative cloud frequency by ISCCP cloud type for the TWP region comparing the ISCCP data in red and the VIRS retrievals in blue.

stratocumulus regime is the dominant cloud mode in both cases, representing more than half of all fields of view. Relative to ISCCP derived optical depths, the optimal estimation method tends to estimate more optically thin clouds and fewer optically thick clouds.

Cloud amounts for the TWP region are presented in table 4.2. Given the limited number of cases, the agreement is excellent, especially for low and middle clouds. The greatest differences are found in the high clouds where the ISCCP climatology suggests more deep convective scenes and fewer cirrostratus clouds than the VIRS data. The cause of this disparity is most likely attributable to effects introduces by differences in spatial resolution, viewing geometry, statistics, and retrieval methodology. For example, the ISCCP data from the GOES satellites is at a lower spatial resolution and some scenes are handicapped by large viewing angles, unlike the higher resolution/nadir looking VIRS retrieval. In addition, the subset of all cloud scenes observed by the VIRS may not be representative of the total population and

differences associated with independent cloud property retrieval methods may worsen comparisons.

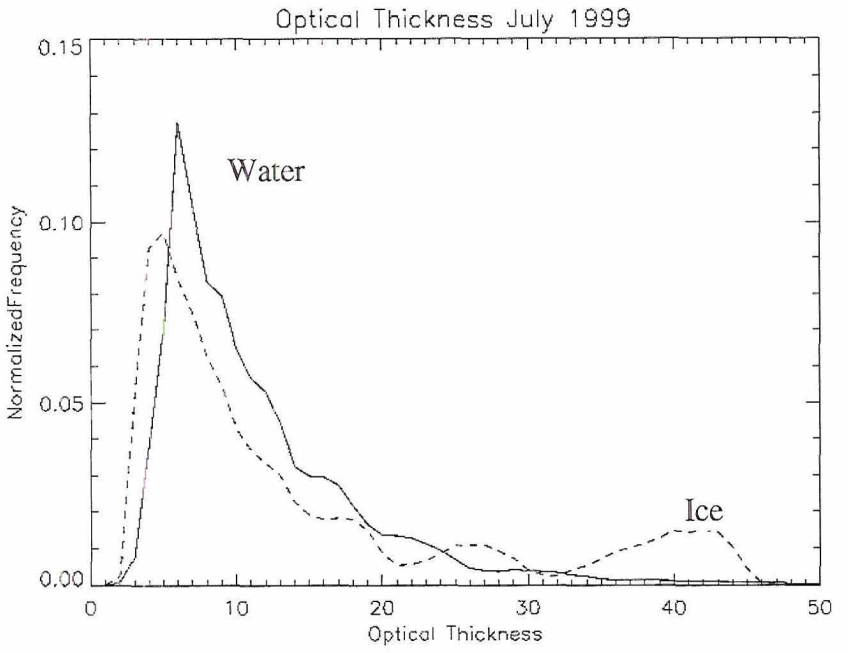

Figure 4.2: Optical thickness histograms of ice and water clouds for July 1999 for the entire TRMM region.

A more detailed examination of the optical depth and height distributions found in this study has yielded some interesting insights. The complete histogram of optical depths found for water and ice clouds retrieved from the VIRS data during July 1999 is presented in figure 4.2. Water clouds show a maximum at small values near $\tau = 5$ with frequencies that fall off monotonically toward higher optical thicknesses. The location of this maximum near an optical depth of 5 is of questionable significance since clouds of smallest optical thickness, less than about 3.0, were eliminated using a visible brightness threshold. Furthermore, water clouds with very small optical depths tend to be of small aerial extent and therefore would not likely fill the VIRS field of view (FOV), leading to a beam filling problem that introduces error in the forward

model. It is likely that the increase of cloud frequency with decreasing optical depth extends to somewhat smaller values of τ than is represented here. However, this determination cannot be made with the current retrieval nor with an instrument of the current horizontal resolution of 2 Km.

The histogram of ice cloud optical depths also contains some interesting features. The issues at the smallest depths discussed above in relation to the water clouds still remain. In addition, the ice cloud distribution contains the added complexity of multiple maxima at the higher optical depths. The maximum centered near an optical depth of 40 is most likely associated with deep convective towers. Although the actual optical depths of these clouds are on the order of hundreds or thousands, values of this magnitude cannot be accurately retrieved since the modeled radiances approach saturation rapidly for optical depths near 40. Other maxima in the distribution, at optical depths near 25 for example, are most likely explained by thick cirrus decks generated by the deep convective clouds.

Figure 4.3 is a plot of relative cloud frequency as a function of height and optical depth for the entire TRMM region for July 1999. Two features of this distribution are striking. First, low optical thickness clouds are abundant at all levels. Second, there are a large number of low water clouds, which are very common up to optical depths of roughly 25. These signatures are likely the result of the ubiquitous cirrus and boundary layer cumulus clouds, and low-level stratus decks respectively. More subtle, are the two higher concentration regions in the upper troposphere (e.g. between 6-12 Km) near optical depths of 25 and 40 that represent the secondary ice optical thickness peaks discussed above. The higher optical depth regions are

associated with deep convection, while the smaller optical depth cases appear to represent a distinct mode of cloud, perhaps thick cirrus layers produced by convective towers. This cirrostratus cloud mode is more evident in figure 4.4, which isolates only ice clouds for July 1999. This figure also shows that the most common height for cirrus to be between 6 and 8 Km, deep convective cloud tops between 5 and 14 Km, and the thicker cirrus mode is most commonly found at 8 to 12 km in height.

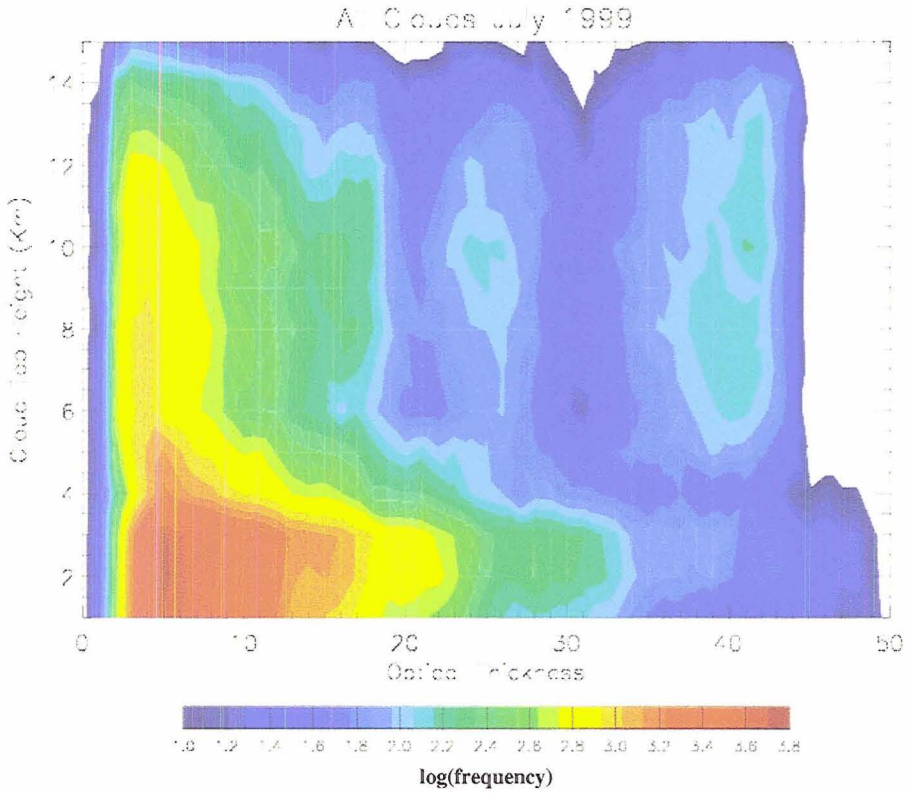

Figure 4.3: Cloud optical depth and cloud top height joint frequency diagram for all clouds over the oceanic TRMM region July 1999.

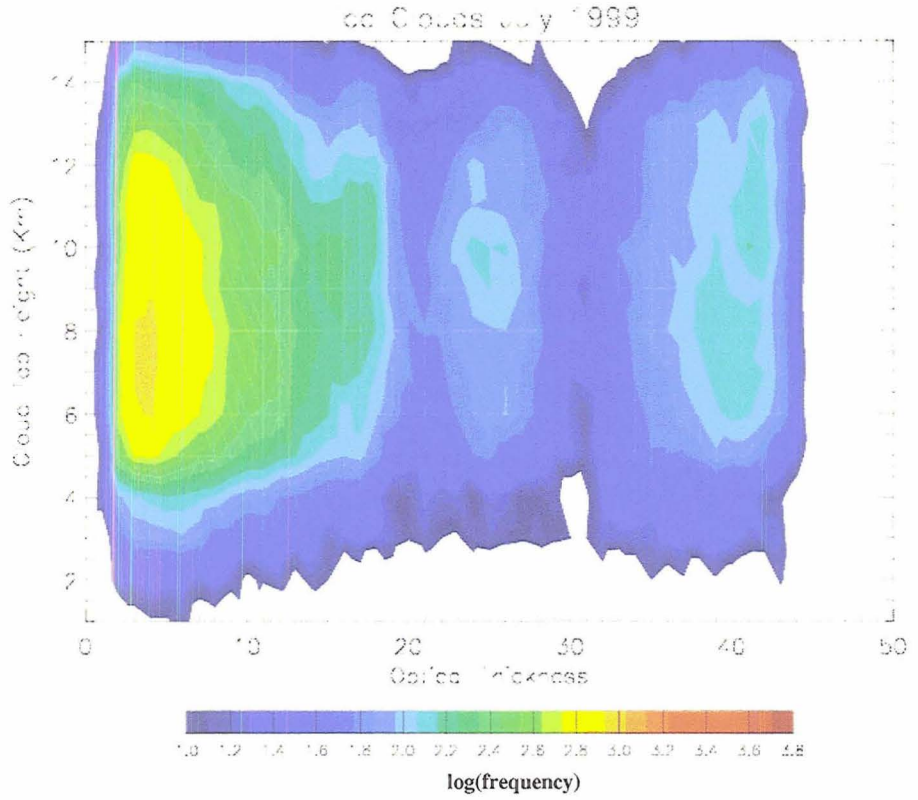

Figure 4.4: Cloud optical depth and cloud top height joint frequency diagram for ice clouds over the oceanic TRMM region July 1999.

Figures 4.5 and 4.6 contain distributions of cloud top heights and optical thicknesses for the TWP region. Here, there are very few water clouds with optical thicknesses in excess of optical depth 10, in stark contrast to the larger TRMM region. This is due to the fact that the large low stratus decks found in certain parts of the world are, by and large, not present in the tropical warm pool region. It should be noted as well that water clouds of all optical thicknesses in this region are likely underestimated due to large high cloud frequencies that effectively mask the existence of underlying water clouds in many instances.

In figure 4.6 we see that although in an area weighted sense there are more deep convective clouds and associated thick cirrus anvils in the TWP region relative to the rest of the globe, they are dwarfed by comparison in this region by the extremely

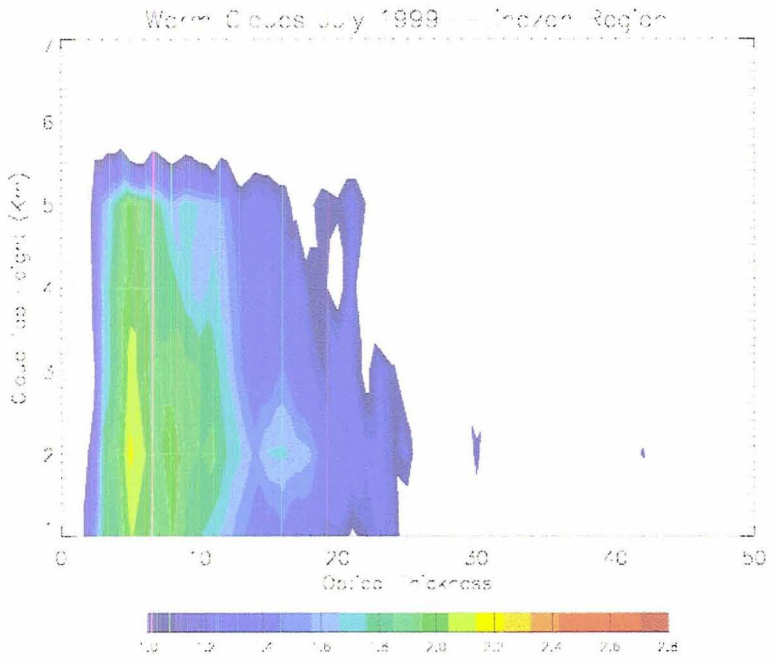

Figure 4.5: Cloud optical depth and cloud top height joint frequency diagram for water clouds over the oceanic TWP region July 1999.

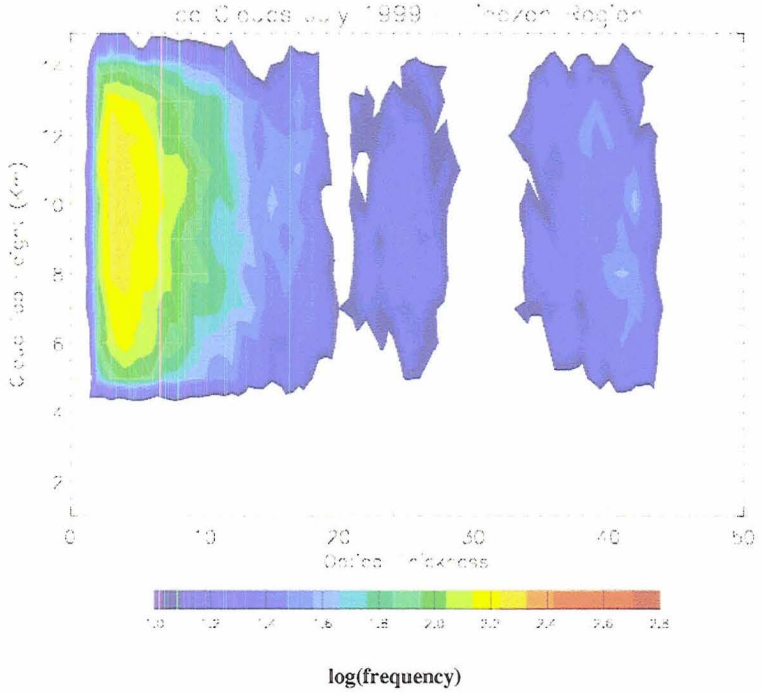

Figure 4.6: Cloud optical depth and cloud top height joint frequency diagram for ice clouds over the oceanic TWP region July 1999.

widespread thin cirrus clouds. Also of note in the TRMM region, the median cloud top height for thin cirrus was 6-8 Km, while in the TWP cirrus cloud top heights are most common between 8 and 12 Km.

4.4 All Cloud Tau - R_e Distributions

The joint distribution of optical thickness and effective radius for warm cloud scenes observed during July 1999 for the entire TRMM region is shown in figure 4.7. In general, the distribution of both parameters is quite smooth, with similar lognormal or gamma-like histograms. The optical thickness frequency peaks near $\tau = 5$ with few values larger than 25, similarly the effective radius frequency peaks near 10 microns and falls off smoothly, with few values in excess of 30 microns. An interesting feature present in this distribution is the cluster of solutions with effective radii of roughly 2 microns and small optical thicknesses. This appears to be the result of a lack of uniqueness and parameter sensitivity in this region of the τ/r_e solution space (figure 3.1). For optical depths less than 3, there is virtually no particle size sensitivity in the near-IR and reflectances do not monotonically decrease with increasing particle size. It may very well be impossible to retrieve cloud particle sizes with a visible/near-IR spectral pair below an optical thickness of approximately 3.

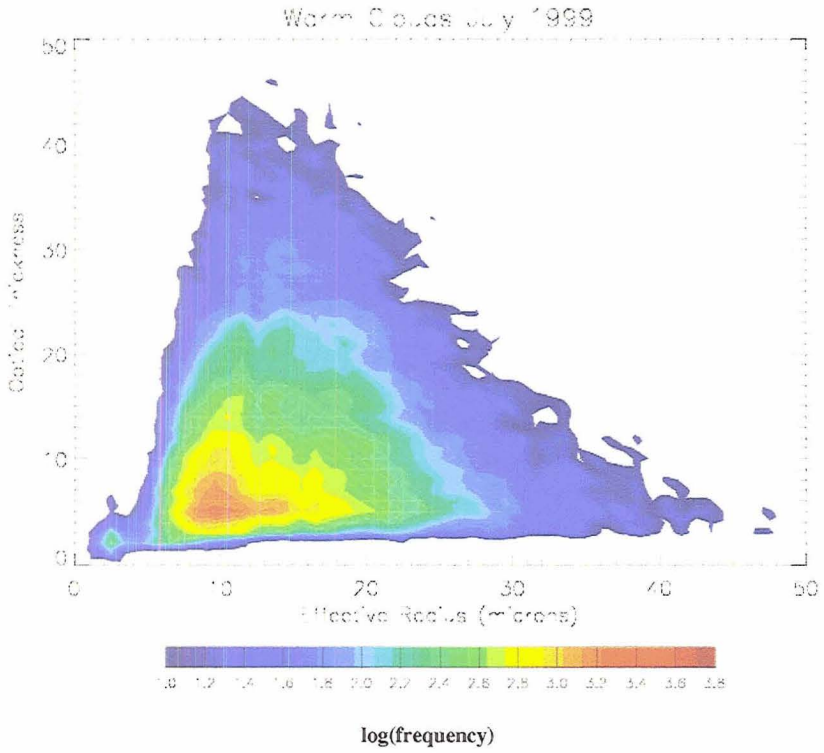

Figure 4.7: Joint distribution of effective radius and cloud optical thickness for water clouds in the TRMM region July 1999.

In this region where the solutions are not unique, the inversion problem is not well posed and the details of the *a priori* assumption and the minimization procedure define the solution as much or more than the physics of the problem. As a result, these retrievals are discounted as unphysical.

The τ versus effective diameter distribution for ice clouds in the TRMM region for July 1999 is presented in figure 4.8. Here we see that the 3 optical depth modes for ice clouds discussed above each exhibit a distinct particle size distribution. The optically thin cirrus clouds have a broad size distribution with common effective diameter values ranging from 20 to 70 microns, with a median value of approximately 45 microns. The more optically thick cirrus as well as the deep convective clouds, on the contrary, have narrower particle size distributions with larger median values in the vicinity of 55 microns.

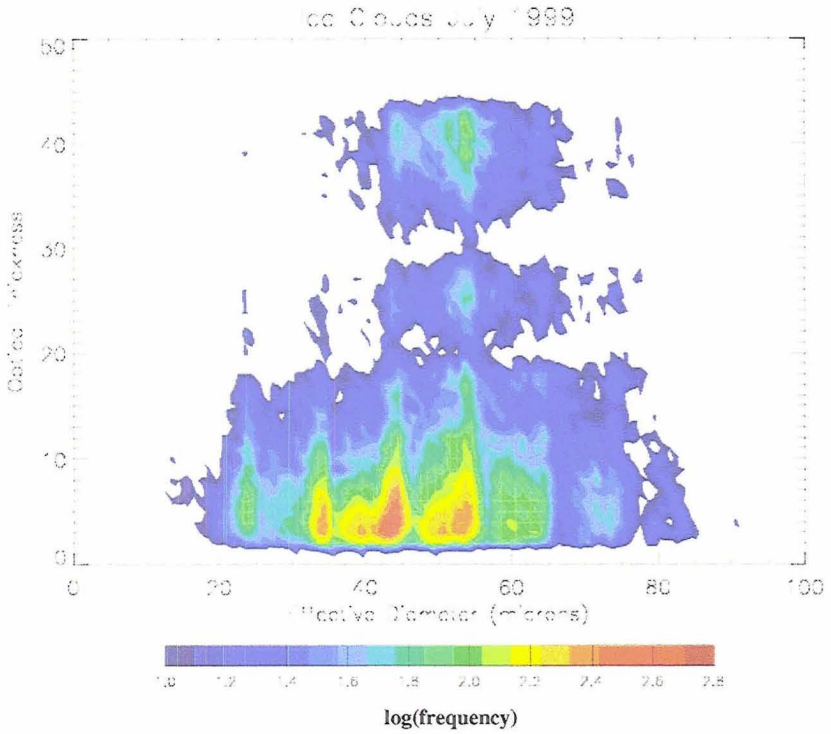

Figure 4.8: Joint distribution of effective radius and cloud optical thickness for ice clouds in the TRMM region July 1999.

4.5 The Role of the A Priori Assumption

It is evident from the ice cloud particle size distribution that there is a tendency for the retrieved particle sizes to be more common at 10-micron intervals, (ie. at 25μ, 35 μ, etc.) Recall, that the ice particle scattering phase functions were provided by MODIS and were discretized at 10 micron intervals in effective diameter. Therefore, the phase function appropriate for 30 microns was applied to all forward model calls with particle sizes between 25 and 35 microns, for example. As a result of this constant phase function assumption, the sensitivity of the radiance field to changes in particle size is artificially reduced due to the constant asymmetry parameter assumption imposed on the solution space. This leads the inverse procedure to lend more weight to the *a priori* particle size assumption than it ideally should. Due to this unexpected numerical artifact it is desirable to determine what fraction of the

information in the retrieved solution comes from the measurement data relative to the *a priori* assumption.

The averaging kernel or "A-matrix" provides precisely that. A-matrix values near unity imply that the retrieval is by and large ignoring the *a priori* value and instead utilizing measurement data. Smaller values of the A-matrix imply that the *a priori* assumptions are driving the retrieval solution, therefore negating their physical significance.

The calculated "A-values" for both the particle size and optical thickness retrievals for water and ice clouds are presented in figures 4.9 - 4.12. It is evident that the water cloud retrievals are, by and large, well posed. The *a priori* assumption only plays a significant role for τ determination at large optical thicknesses and particle size determination at very small r_e. Similarly, τ determination in ice clouds is primarily measurement driven except at large optical depth. However, the ice particle size retrievals shows excellent measurement sensitivity near the phase function "breaks", and poor measurement sensitivity in between, especially at small optical depths.

Using a more detailed 1-μ resolution phase function space on a small number of orbits, ice particle size distributions, not shown, are overall very similar but do not exhibit the banding procedures observed above. Further, A-matrix analysis indicated values above .95 for particle size determination for sizes less than $D_e \sim 80$ microns.

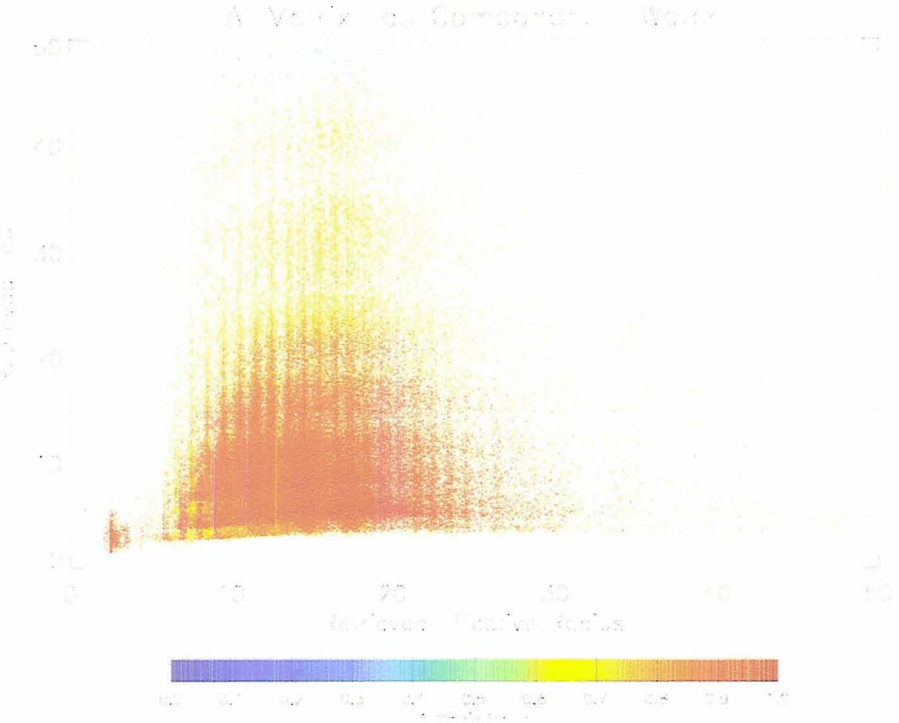

Figure 4.9: A-matrix optical thickness component for retrieved water clouds from July 1999.

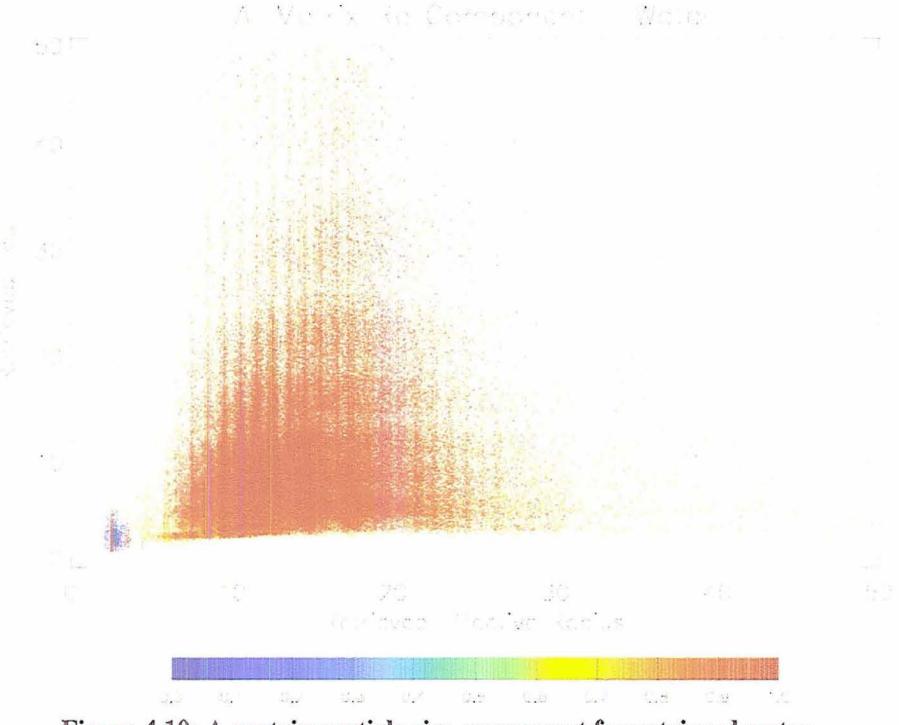

Figure 4.10: A-matrix particle size component for retrieved water clouds from July 1999.

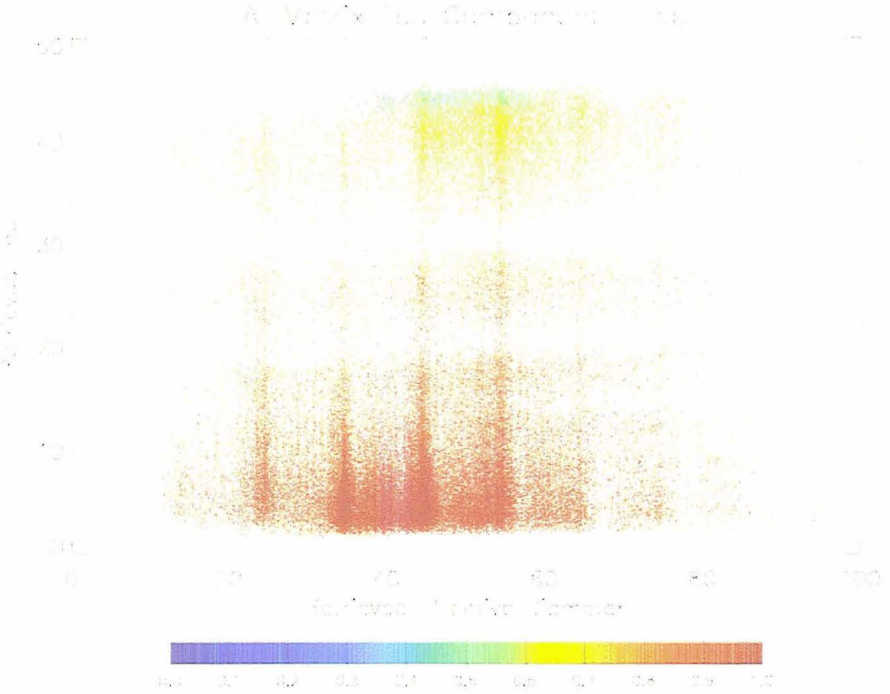

Figure 4.11: A-matrix optical thickness component for retrieved ice clouds from July 1999.

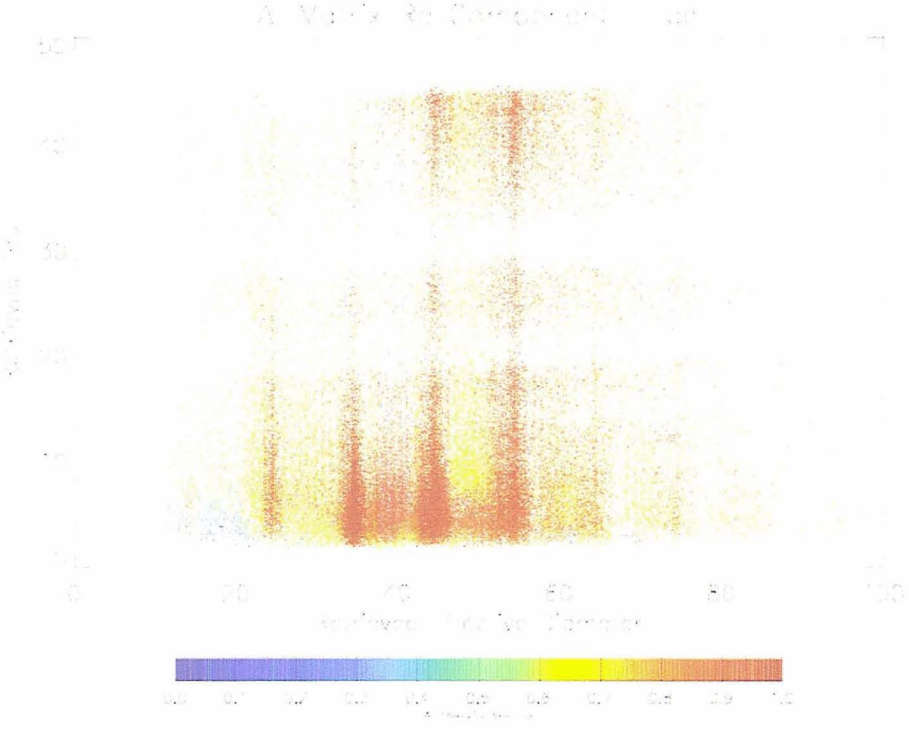

Figure 4.12: A-matrix particle size component for retrieved ice clouds from July 1999.

4.6 Examining Precipitating Clouds

Both the PR and the TMI incorporate methods to determine whether a particular field of view (FOV) is likely to contain a precipitating cloud, however, each uses completely independent approaches to arrive at this determination. The PR uses an active microwave system and a noise correction algorithm to determine whether precipitation sized particles are likely in each range gate. On the other hand, the TMI 2A12 algorithm uses a large library of cloud resolving model simulations that are designed to span the physical realm of observed clouds. It then identifies the pre-calculated cloud scene that best matches the 5 passive microwave observations. The rain rate is determined by a weighted average of a number of the most consistent cloud profiles, this number is then ascribed to the scene within the FOV.

For this study, each converged cloud particle size and optical depth retrieval from the VIRS instrument is collocated with the appropriate TMI and PR footprint to obtain 2 independent estimates of rainfall. Precipitation in this study is treated as a binary process, where cloud pixels that contain precipitation sized particles at any level in the column are considered precipitating. Correlations of effective radius and optical thickness as a function of rainrate and elevation are subjects of future work.

During July 1999 in the TRMM region approximately 5.7% of water clouds cases were determined to contain precipitation by the TMI and 3.6% by the PR. Of all ice clouds observed by the TMI 24.7% had precipitation compared to 23.1% of cases observed by the PR. In terms of identifying precipitation the PR is considered the superior instrument (Kumerrow personal communication). This coupled with its

higher spatial resolution made PR data the data of choice in the analysis that follows unless otherwise stated.

Figure 4.9 presents the raining and non-raining cloud top effective radius histograms normalized by total number of cases for the TRMM regions during July 1999. The two distributions are distinct: precipitating clouds have a median value of 19.51 microns with a standard deviation of 7.51, whereas non-raining scenes have particle sizes of 10.65 microns in the median with a standard deviation of 5.77. Rosenfeld and Lemsky (1998) suggest an effective radius of 14 microns, (the vertical line in figure 4.9), as an appropriate threshold to discriminate precipitating clouds. The current results suggest that the use of this 14-micron value is a simplistic threshold for precipitation owing to the significant overlap in the solutions. The most that can be said with confidence is that water clouds with effective radii less than approximately 12 microns are almost certainly not raining, while clouds with cloud top effective radii greater than 30 microns almost certainly contain precipitation sized particles.

It is also of interest to note that the effective radius histogram for non-raining clouds has a significant secondary peak near 15 microns. It is likely that this is due to a mode of lightly raining or drizzling clouds in which the rain rates were too small to be discriminated by the precipitation radar; this supports the use of 14 microns perhaps as a better threshold to discern drizzle containing water clouds in a stratocumulus regime.

Figure 4.10 is a joint probability distribution of retrieved optical thickness and effective radius for precipitating water clouds in the TRMM region during July 1999.

Comparing this to figure 4.7, which represents water clouds, there is a marked shift to both larger particle sizes, discussed above, and to larger optical depths, likely the result of the precipitating clouds being more vertically developed. In this case, the mean optical thickness has increased from 8.57 for non-raining clouds to 15.05 in the raining clouds.

Also of note, for precipitating water clouds it is shown that cloud top particle sizes are positively correlated with optical thickness. This is in direct contrast with the results of Nakajima and Nakajima (1995), who suggest a negative correlation for raining warm clouds. This relationship, which is examined further is section 4.7, could have implications in the area of aerosol indirect forcing of cloud radiative properties.

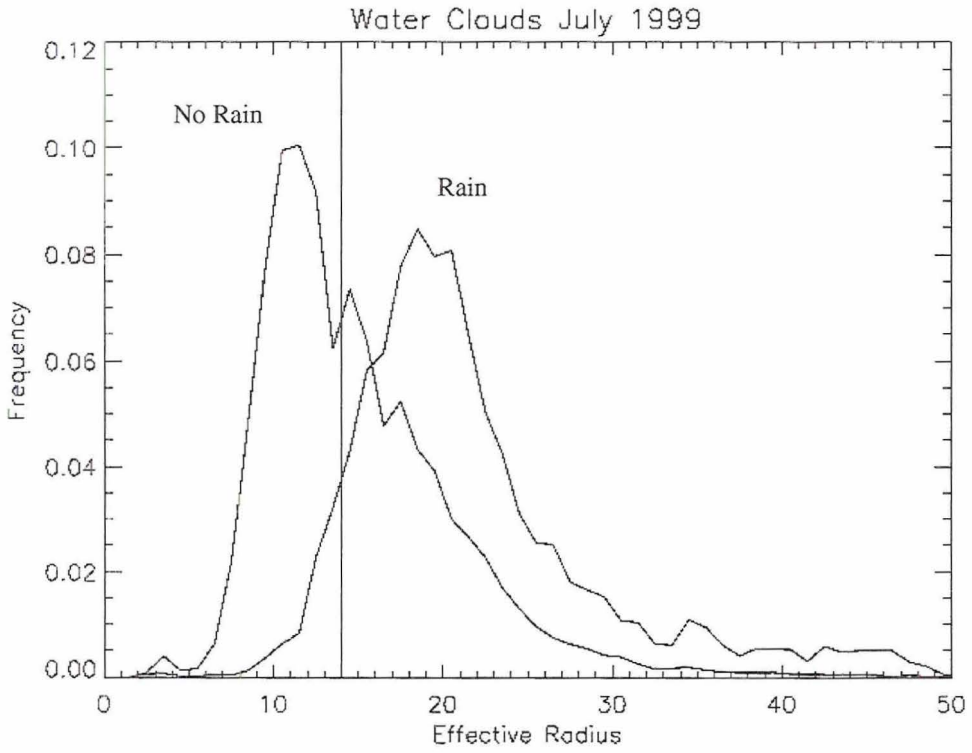

Figure 4.13: Histograms of cloud top effective radius for al water clouds identified in the TRMM region, July 1999.

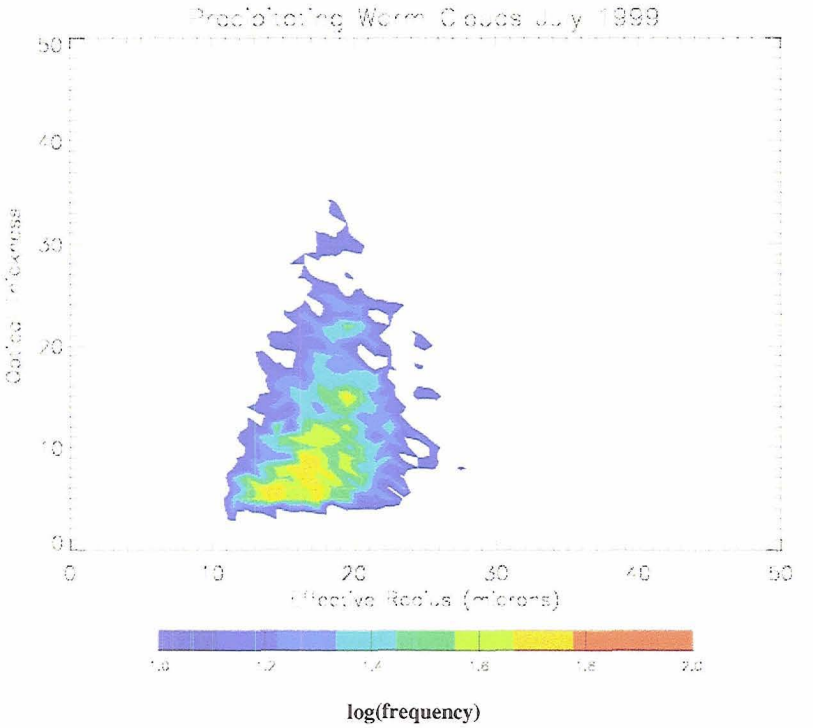

Figure 4.14: Joint distribution of effective radius and cloud optical thickness for precipitating water clouds in the TRMM region July 1999.

In the water cloud case, a significant statistical increase in both the particle size and optical depth in the precipitating cases is observed, however there was no general regime shift in the height distribution or morphology of the precipitating clouds relative to non-raining cases. Therefore, it is conjectured that the observed particle size increases are due to microphysical changes occurring within the clouds as precipitation develops and not due to the appearance of a distinct cloud mode. In the ice case, a sizeable increase in the mean particle size is also observed in the precipitating cases. However, in contrast to the water cloud case, this increase is spurious in the sense that it does not appear to represent a microphysical change within the clouds as precipitation develops, but rather is due to the fact that the optically thin cirrus clouds, characterized by smaller particle sizes almost universally are non-precipitating, while the more optically thick deep convective clouds

overwhelmingly dominate the precipitating cloud population and, on average, contain larger cloud particles (Figures 4.11, 4.12).

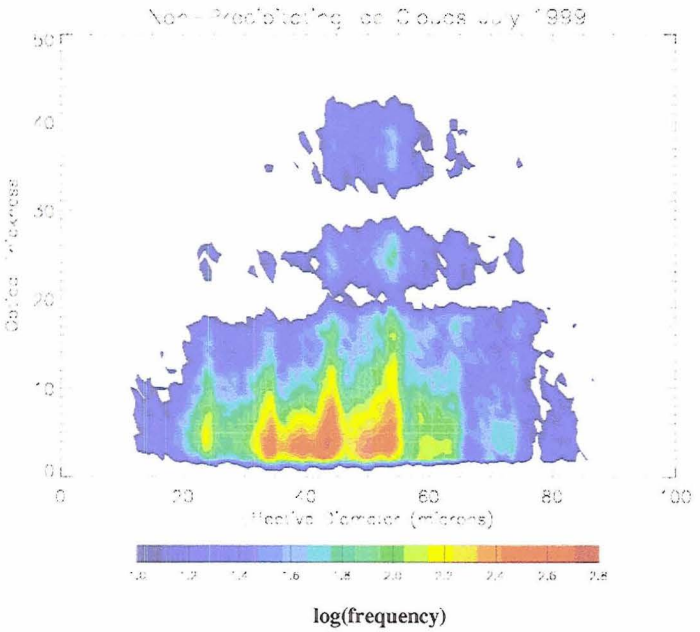

Figure 4.15: Joint distribution of effective radius and cloud optical thickness for non-precipitating ice clouds in the TRMM region July 1999.

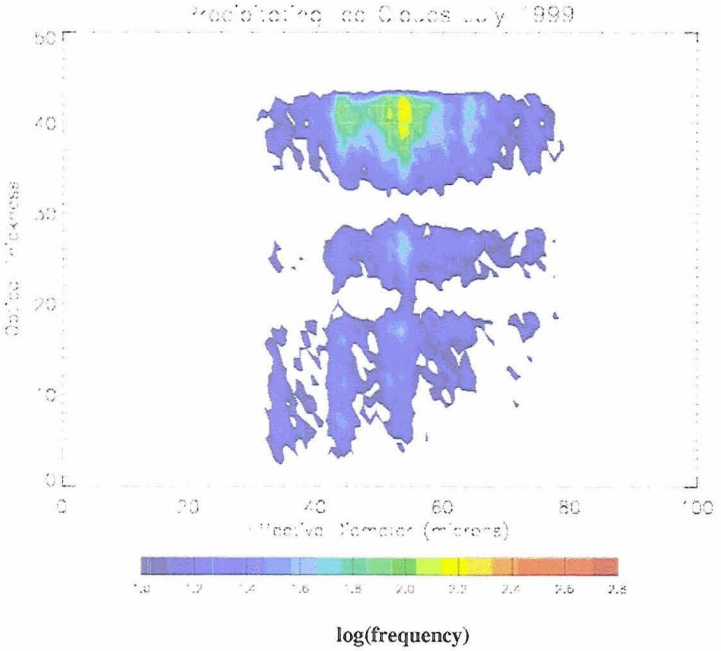

Figure 4.16: Joint distribution of effective radius and cloud optical thickness for water clouds in the TRMM region July 1999.

Water Clouds R_e

Case	Median (microns)	Std. Dev.
PR non-raining (NR)	13.25	5.77
PR raining (R)	19.51	7.51
TMI (NR)	13.05	5.76
TMI (R)	19.05	6.80

Water Clouds Tau

Case	Median	Std. Dev.
PR non-raining (NR)	8.57	6.54
PR raining (R)	15.05	10.49
TMI (NR)	8.50	6.43
TMI (R)	13.91	10.14

Ice Clouds D_e

Case	Median (microns)	Std. Dev.
PR non-raining (NR)	46.91	14.17
PR raining (R)	53.96	13.56
TMI (NR)	47.52	14.30
TMI (R)	52.94	13.75

Ice Clouds Tau

Case	Median (microns)	Std. Dev.
PR non-raining (NR)	7.44	8.75
PR raining (R)	34.30	12.38
TMI (NR)	7.41	9.33
TMI (R)	27.49	12.96

Table 4.3: Median optical thickness and effective radius values derived by the OE retrieval from July 1999.

4.7 Spatial Effective Radius Patterns

Figures 4.13 and 4.15 preset spatial maps of retrieved effective radius from the optimal estimation VIRS retrieval for July and January 1999 respectively. The mean value for each 2.5-degree box is plotted. This resolution was selected such that virtually every grid box contained at least 50 observations, with some approaching 500. This insured robust statistics. Only water cloud particle sizes are plotted to avoid problems with incorporating ice particle data with different units, and to isolate those clouds which are most likely affected by aerosol and cloud condensation nuclei (CCN) concentrations. Figures 4.14 and 4.16 present the mean retrieved effective radius from the operational MODIS data using data collected aboard the TERRA platform for July and January 2000. What is immediately evident is that while many of the large-scale spatial patterns agree quite well, the MODIS product significantly

overestimates particle size relative to the optimal estimation data. In addition, while the spatial patterns appear similar, figure 4.17 which presents the oceanic zonal averages of retrieved effective radius, implies that there are significant differences between the VIRS derived values of effective radius and the MODIS values; both schemes show the particle sizes in July to be larger than those in January at nearly all latitudes. However, the MODIS retrieval shows virtually no zonal variation and greater seasonal variation in the Northern Hemisphere, while the OE retrieval exhibits a good deal of zonal structure and greatest seasonal variability south of the Equator. It is not clear to the investigator what distinct aspect of the retrievals would lead to these significant physical differences.

Another study carried out by Han and Rossow (1993), attempted global effective radius retrievals of water clouds using Advanced Very High Resolution Radiometer (AVHRR) data from January and July of 1987. Their retrieval approach differed from the current optimal estimation approach in several important ways. First, they employed a 2-channel look up method using a visible (0.6-μ) as well as a shortwave-IR (3.7-μ) band, that, while similar to the MODIS implementation, is more complicated due to it's inclusion of cloud height, cloud top temperature, and optical thickness information derived by the ISCCP program. As a result on this reliance on the ISCCP data, the retrieval is performed using radiances sampled to a 30 Km by 30 Km footprint. Further, the McClatchey climatological representations are utilized as the model atmospheres (McClatchey 1972), as opposed to the NCEP "observed" atmospheres employed in the OE VIRS retrieval.

Despite these differences, the two retrieval schemes arrive at similar cloud top effective radii, at least in a statistical sense. For oceanic water clouds, Han and Rossow arrive at a mean particle size of 11.8 microns, with a standard deviation of 5.6, while the OE VIRS retrieval finds a mean particle size of 13.2 microns with standard deviation 5.7. The most likely explanations for the observed difference between these two data sources are the fact that different spatial domains are considered in the two studies, and the fact that the AVHRR retrieval derives its particle size information from the 3.7-micron channel, which was shown in section 3.2 to, on average, imply smaller particle sizes than either the 1.63 or 2.13 microns channels. Despite the global bias, the zonal effective radius structure inferred from the AVHRR contains more zonal structure than the MODIS values and is in better agreement with the OE VIRS retrievals. Figure 4.18 presents the zonal mean particle sizes found by the AVHRR team compared with the OE VIRS averages. The VIRS zonal means presented here differ from those found in figure 4.17, due to the implementation of different averaging procedures used to recreate the analysis performed by MODIS and Han and Rossow in each case. Though the details of the zonal structure differ, the AVHRR and VIRS data are similar in the sense that both schemes infer larger particle sizes in July relative to January, both show relative minima near the equator and maxima in the sub-tropical regions, and both show a large seasonal shift in the Southern Oceans, with the largest differences located at roughly 30^{o} south.

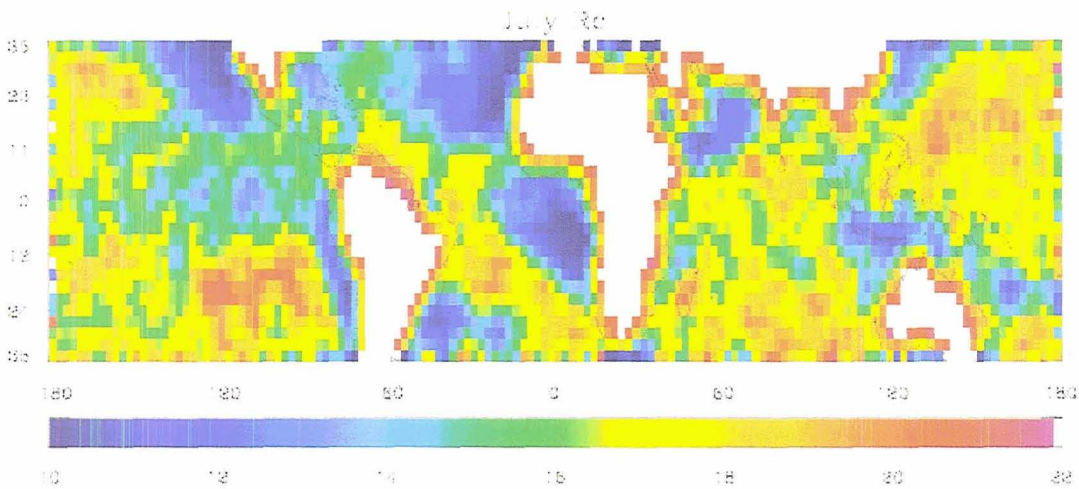

Figure 4.17: Mean effective radius in microns from the optimal estimation VIRS retrieval, July 1999. Data are gridded at 2.5 x 2.5 degree resolution.

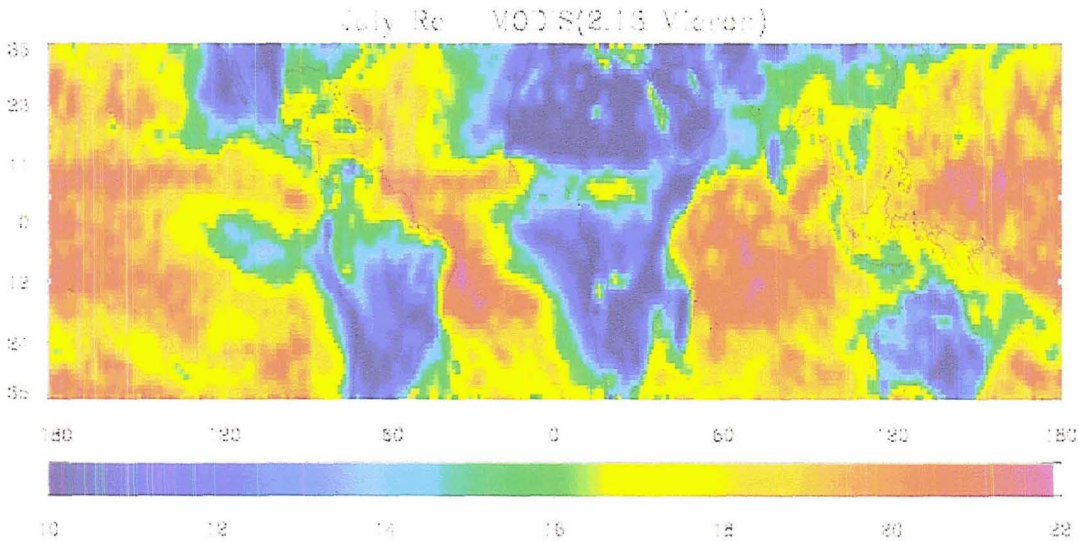

Figure 4.18: Mean effective radius in microns from the operational MODIS retrieval, July 2000. Data are gridded at 1.0 x 1.0 degree resolution.

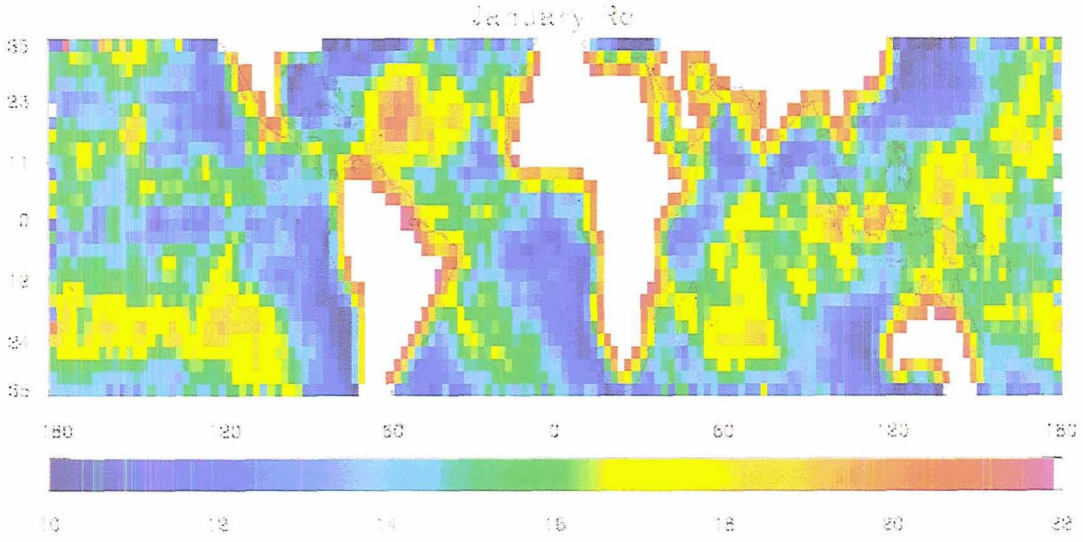

Figure 4.19: Mean effective radius in microns from the optimal estimation VIRS retrieval, January 1999. Data are gridded at 2.5 x 2.5 degree resolution.

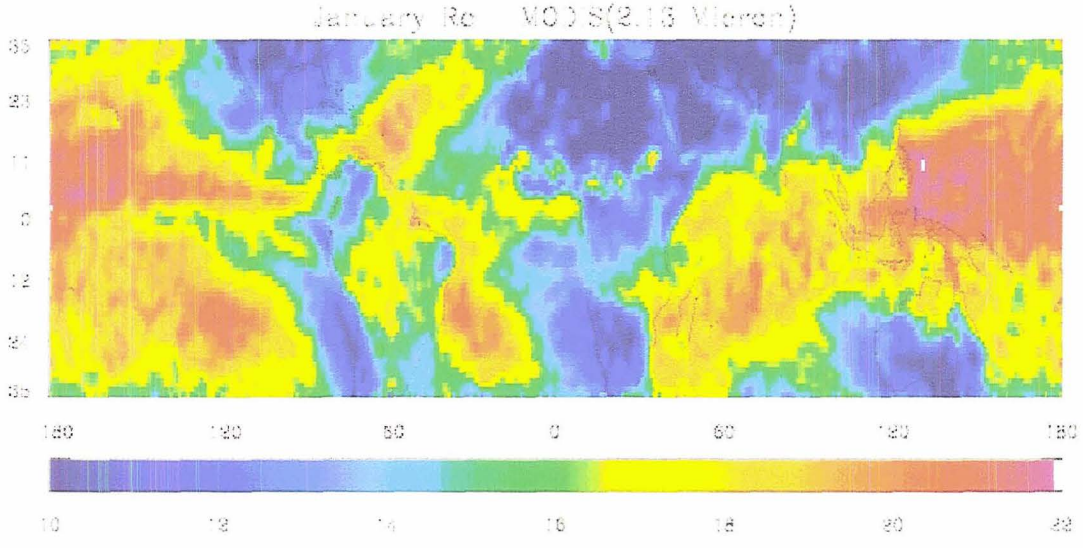

Figure 4.20: Mean effective radius in microns from the operational MODIS retrieval, January 2000. Data are gridded at 1.0 x 1.0 degree resolution.

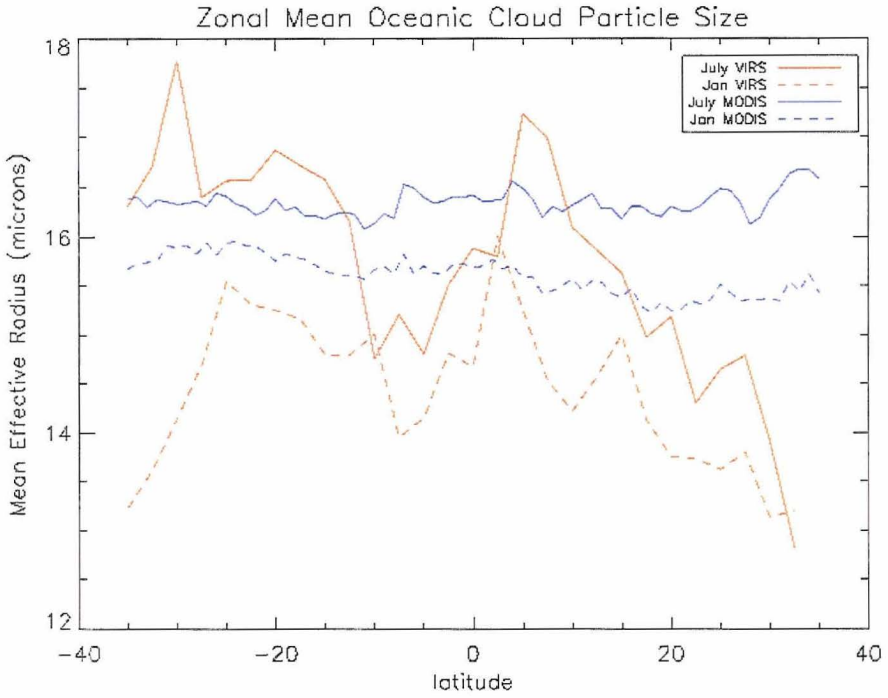

Figure 4.21: Zonal means of retrieved effective radius from oceanic pixels for the operational MODIS and optimal estimation VIRS retrieval from January and July.

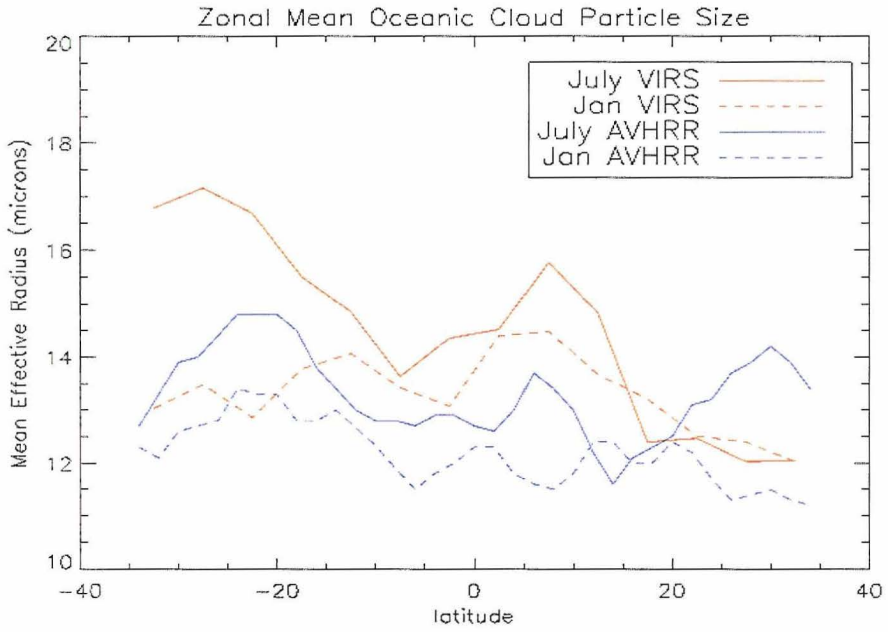

Figure 4.22: Zonal mean of retrieved effective radius from oceanic pixels for the optimal estimation VIRS retrieval from January and July 1999. A distinct averaging technique was used from the previous analysis to match AVHRR methodology.

Figures 4.20 and 4.21 are monthly averages of aerosol optical thickness for January and July 1999 from retrievals performed using the NOAA-14 AVHRR instrument. The data are at 100 Km resolution and are used here as a proxy for boundary layer CCN concentrations. These concentrations are of interest because it is theorized that increases in CCN will lead to reductions in water cloud particle sizes, due to the fact that larger nuclei concentrations are thought to increase the number of cloud particles without affecting the cloud's liquid water content (Twomey 1980). This so-called aerosol indirect effect is a current area of research in the climate change community due to the fact that reductions in cloud particle size can act to increase the cloud's overall albedo and can further act to reduce precipitation efficiency (Khain et al. 2004) (Ziegler 1988).

The particle size spatial distributions contain several striking features. First, in the July data and to a lesser degree in January, the predominate stratocumulus regions off the west coasts of North and South America, as well as Africa, exhibit well defined regions of small particle sizes. This is due to the fact that these areas are characterized by widespread regions of shallow water clouds with very modest vertical velocities, resulting in relatively small cloud top particle sizes.

In July, the clouds in the southern oceans are found to have large median effective radius values of 16-18 microns, while in January these same regions have somewhat smaller ~13 micron particle sizes. These changes correlate well with the observed aerosol optical thicknesses. In July, the southern oceanic air is seen, in figure 4.15, to be nearly devoid of aerosol, with most regions characterized by AOTs of less than .4, whereas in January typical values are 3 –5 times as large. The effective radius results

are in agreement with results obtained from the Southern Ocean Cloud Experiment (SOCEX), which occurred in Southern Australia in 1995. Through in-situ observations, this study found that in the pristine air of the Southern Ocean was characterized by a distinct seasonal cycle of non-anthropogenic aerosol concentrations, whose source is oceanic dimethyl-sulphide (DMS). Boers et al. (1996) observed very low droplet concentrations of roughly 30 cm^{-3} in the boundary layer with typical effective radii of 16 to 18 microns. Summer-time droplet concentrations were 3-fold larger with particle sizes in the 12-14 micron range. These SOCEX results suggest that the OE VIRS data better matches the observed Southern Ocean data than does either the operational MODIS retrieval or the AVHRR results of Han and Rossow (1993).

While this is the most dramatic example, other areas of aerosol influence can be seen. Large aerosol optical depths found in the Arabian Sea in July as well as off the coast of China in January are also shown to correlate well with areas of reduced cloud top particle sizes.

While this work represents only a cursory initial look at the effect of aerosols on water cloud particle sizes it will hopefully, in the future, undertake more direct comparisons between the effective radius and optical thickness of individual cloud scenes with collocated boundary layer aerosol data. This type of analysis will be made possible by aerosol profiles produced by the ICESAT satellite program and will be an area of future research.

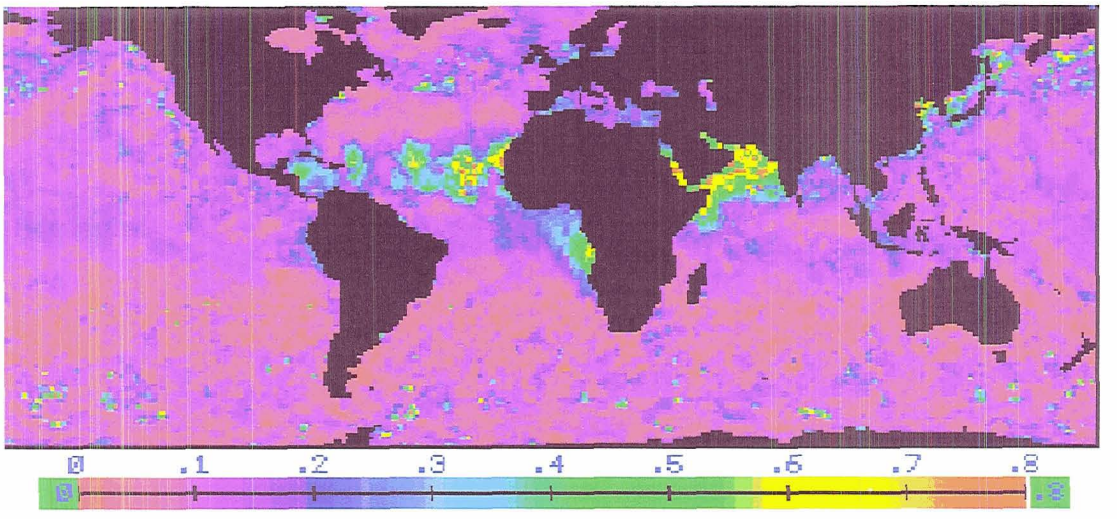

Figure 4.23: Retrieved Aerosol Optical Thickness (AOT) derived from data provided by NOAA/AVHRR satellite. July 1999.

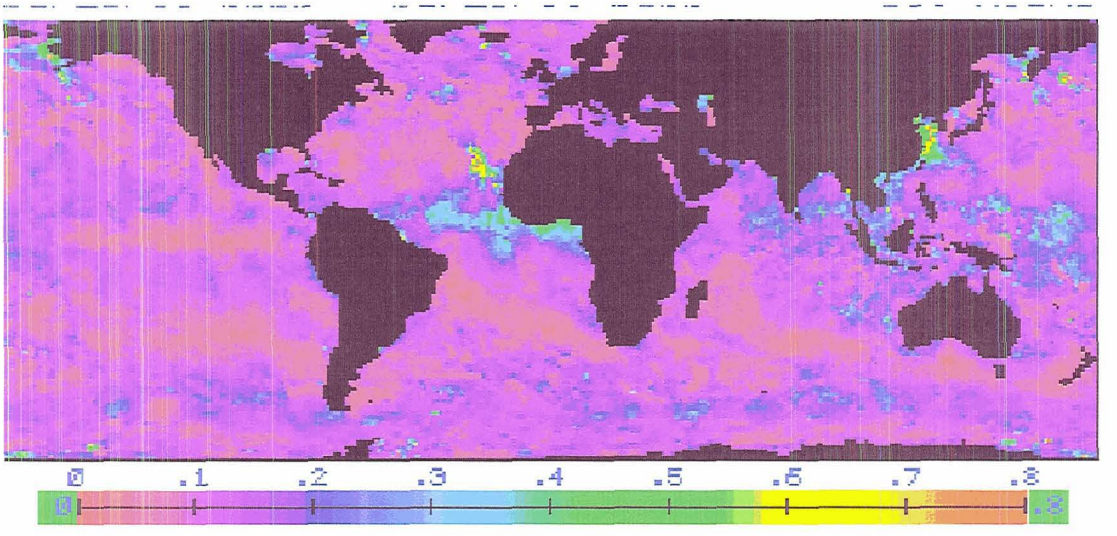

Figure 4.24: Retrieved Aerosol Optical Thickness (AOT) derived from data provided by NOAA/AVHRR satellite. January 1999.

4.8 Tau/R_e Correlations

Nakajima and Nakajima (1995) showed that stratocumulus regions off California characterized by clean maritime air exhibited particle sizes that were negatively

correlated with optical thickness, while in more polluted regions there was a positive correlation between effective radius and measured optical thickness. They argue that in polluted regions, the drizzle process is reduced, resulting in a thickening of the stratus with the most opaque clouds containing the largest particle sizes, while in clean environments the clouds with the largest particle sizes form drizzle, reducing their liquid water path, and therefore their optical depth resulting in the observed negative correlation.

The results presented in this thesis suggest that when this analysis is extended to all water clouds the relationship becomes somewhat more complicated. Figure 4.22 presents the effective radius/optical thickness regressions for water clouds retrieved by the OE VIRS retrieval in July 1999. In general, observed regressions lie between zero and positive 2, with very few of the negative correlations observed by Nakajima and Nakajima. Three regions are highlighted in 4.22 and the scatter plots of optical thickness and effective radius in these regions are presented in figure 4.23. Region 1 is characterized by large positive slopes and relatively large particle sizes, with median values between 15 and 17 microns. It is in a region of relatively pristine air, and has many thick clouds with large particle sizes. This region seems to be very distinct from the stratocumulus observed by Nakajima and Nakajima and is shown by the PR to be a region of frequently precipitating, and likely vertically developed, water clouds. Region 2 is characterized by large positive regressions, small mean particle sizes, between 9-12 microns, and heavy aerosol loading. Its τ/r_e scatter plot is very similar to those observed in the prior study of Nakajima and Nakajima, and is mostly characterized by many optically thick scenes with small particle sizes, a

signature of aerosol-influenced clouds. Region 3 has nearly zero slope, and very large mean particle sizes, approaching 20 microns. Figure 4.23 shows that this region has very few optically thick clouds and very large effective radii. In this relatively clean maritime environment, these clouds are overwhelmingly precipitating, leading to a reduction in liquid water content, thus limiting their optical thickness.

An identical analysis is performed for January 1999 and is presented in figure 4.24, with scatter plots of highlighted regions exhibited in figure 4.25. Slightly negative slopes, moderate aerosol loading, and large median particle sizes characterize region 5. Its scatter plot most closely resembles the negative regression regimes found in Nakajima and Nakajima (1995), with a mix of optically thin precipitating scenes and more opaque aerosol influenced clouds with small cloud top effective radii.

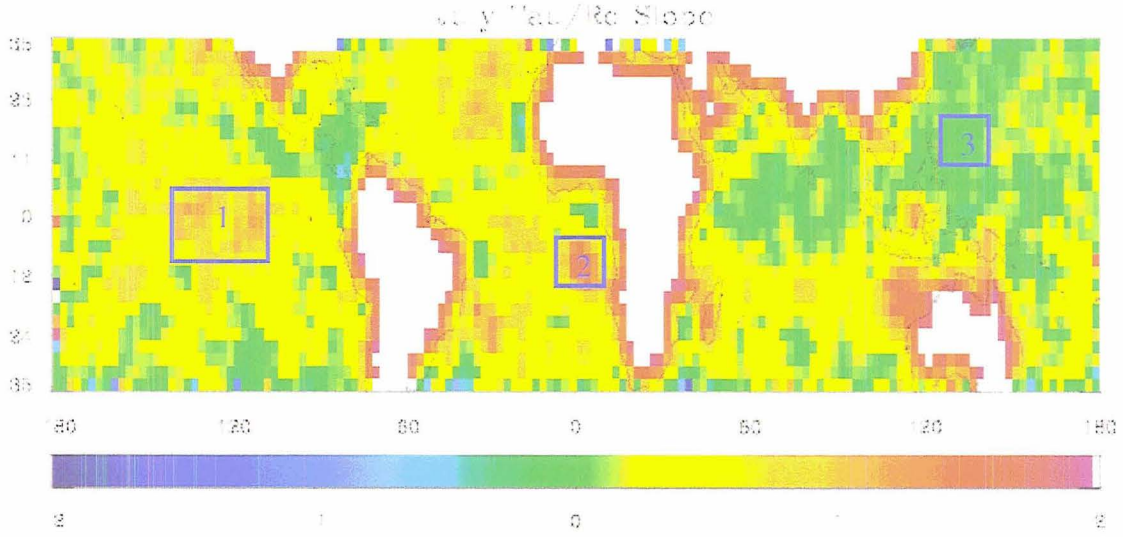

Figure 4.25: Regression coefficients of optical thickness and effective radius for water clouds from the OE VIRS retrieval for July 1999.

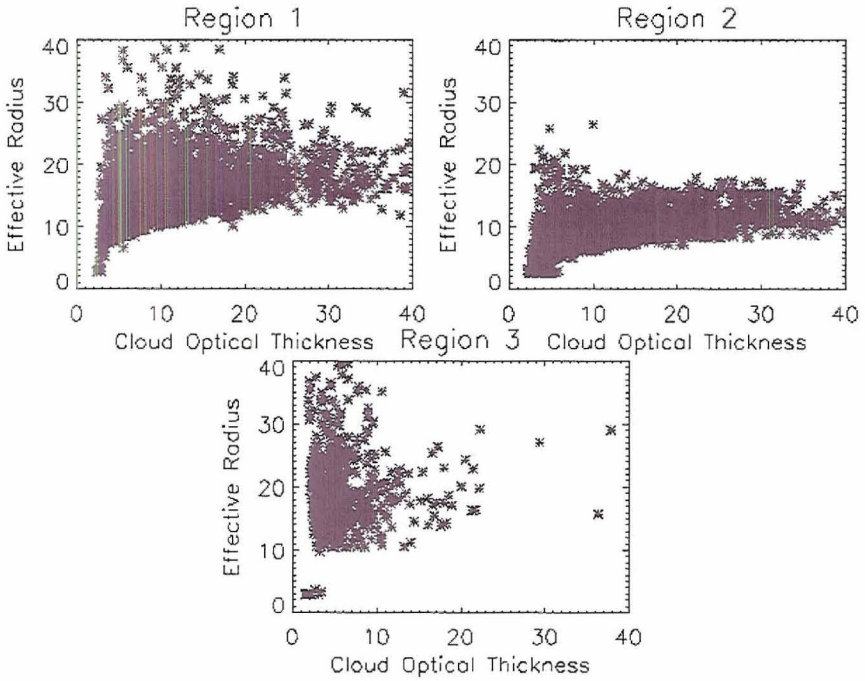

Figure 4.26: Optical thickness and effective radius scatter plots for water clouds retrieved with the OE VIRS retrieval for July 1999 in highlighted regions.

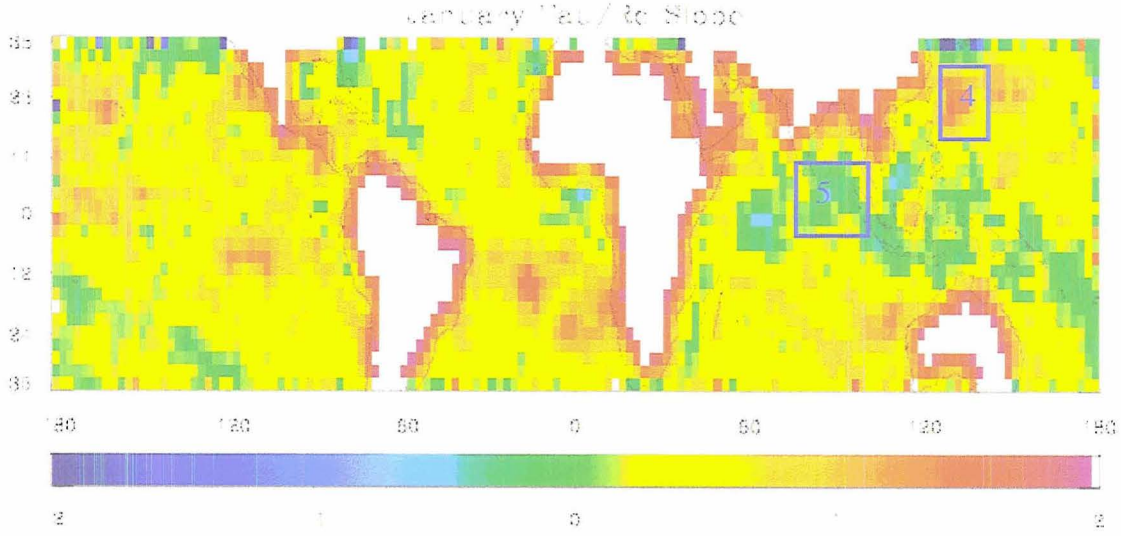

Figure 4.27: Regression coefficients of optical thickness and effective radius for water clouds from the OE VIRS retrieval for January 1999.

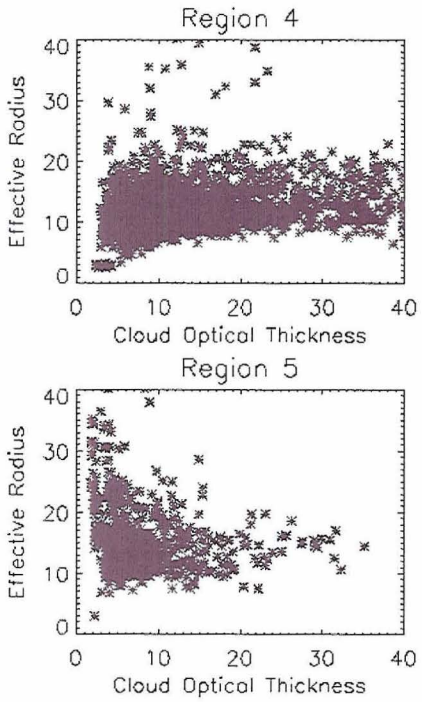

Figure 4.28: Optical thickness and effective radius scatter plots for water clouds retrieved with the OE VIRS retrieval for January 1999 in highlighted regions.

CHAPTER 5: CONCLUSIONS

5.1 Principal Findings

The goal of this thesis was to develop an efficient, research grade 3-channel optimal estimation (OE) cloud top effective radius and optical depth retrieval for the VIRS instrument and to assess its performance through comparison with other data sets.

- Good agreement was found with the operational MODIS particle size retrieval for ice clouds using a simplified 2-channel "MODIS retrieval simulator". When the full 3-channel OE retrieval with explicit errors was compared for the same scene a 15% negative bias was observed in the OE result. The discrepancy was ascribed to the introduction of independent 3.75-μ information, independent radiative transfer implementations, and distinct inversion techniques.
- For water clouds, the OE retrieval was found to produce a 15-45% negative bias in effective radius (r_e) and an 8% positive bias in optical thickness relative to the operational MODIS retrieval. However, when the MODIS simulator OE retrieval was compared, these biases were reduced to 10-25% r_e. The introduction of the 3.75- μ information as the third channel was thought to account for roughly half of the overall discrepancy, with the remainder due to forward model brightness differences resulting from details of the radiative

transfer implementation regarding atmospheric gases and scattering phase functions.

- It is proposed that for the cloud scenes examined, the more fully developed 3-channel optimal estimation approach produces not only different, but superior results. This is due to the fact that more pertinent spectral information is considered; cloud scenes used for comparison were carefully selected to adhere to the forward model's plane parallel assumptions and due to the explicit error characterization provided by the optimal estimation approach.
- Histograms of cloud top height and optical thickness were compared to the International Cloud Climatology Satellite Program (ISCCP) data for the TRMM region as well as the Tropical West Pacific (TWP) region for July 1999. Close agreement was found in both cases, although the OE retrieval characterizes fewer deep convective scenes and more optically thin high clouds than were found by the ISCCP team.
- More detailed optical thickness/cloud top height distributions for ice clouds exhibited a robust tri-modal optical thickness structure, representing cirrus, moderately thick ice clouds, and deep convection, in both the TWP as well as the broader TRMM region
- The 3 ice cloud optical thickness regimes were found to have distinct particle size distributions. Cirrus clouds had typical effective diameter values of 20-70 microns, with a median value near 45, while the thicker ice clouds were characterized by a more narrow size distribution shifted to larger values centered near 55 microns.

- For water clouds, the optical thickness distribution was found to be a very smooth with a peak near $\tau = 5$, though as discussed this peak is considered artificial due to the direct elimination of optically thin clouds and the fact that clouds with small optical depths are typically very small in aerial extent and therefore may not completely fill a VIRS FOV. Further, few water clouds with optical thickness in excess of 25 in the TRMM region and 10 in the TWP were found. The clouds also exhibited a very smooth effective radius histogram that peaked near 11 microns, with few cases in excess of 30 microns.
- Precipitating water clouds, as determined by the Precipitation Radar (PR), exhibited a very distinct effective radius histogram from non-precipitating scenes, with a median value of nearly 20 microns.
- A secondary maximum at 15 microns in the non-precipitating water clouds may represent a drizzle mode with rainfall too slight to be detected by the PR. These results broadly support the threshold value of $r_e > 14$ microns used to distinguish precipitating stratocumulus cloud scenes by Rosenfeld and Lemsky (1998), but it is shown that the particle size distributions for precipitating and non-precipitating clouds are far from distinct suggesting the role of other mechanisms (i.e. cloud dynamics, turbulence, etc.) besides cloud top particle size in determining the presence of precipitation sized particles.
- For non-precipitating water clouds, effective radius was found to be *negatively* correlated with optical thickness, while in precipitating warm clouds a *positive* correlation was observed.

- Maps of retrieved effective radius for water clouds from the OE VIRS retrieval exhibit similar large-scale structure to the operational MODIS data, but estimate somewhat smaller particles and contain larger zonal and seasonal variations.
- The OE VIRS retrieval compares more favorably with the AVHRR values retrieved by Han and Rossow (1993), however the current study produces particle sizes roughly 15% larger than those inferred from AVHRR.
- Retrieved cloud top particle sizes in water clouds show robust negative correlations with aerosol optical thickness values. This effect is most pronounced in the Southern Ocean where seasonal variations in non-anthropogenic aerosols are shown to result in a 20-30% reduction in cloud top effective radius in January relative to July. This large seasonal effective radius reduction agrees very well with in-situ measurements made during the SOCEX campaign; this seasonal signal is not present in the operational MODIS data.
- Expanding on the work of Nakajima and Nakajima (1995) regressions of optical thickness with effective radius are presented and used to identify a number of regions dominated by distinct water cloud modes, including aerosol influenced water clouds in which there was no drizzle mode, vertically developed precipitating clouds in pristine tropical environments, and an optically thin precipitating mode in regions of very clean boundary layer air.

5.2 Future Work

The current study was limited to cloud optical thicknesses in excess of 3 and to oceanic scenes. It would be fruitful to extend these results globally as well as to more optically thin cloud scenes. However, additional retrieval development would be required to examine optically thin scenes, since there is very little parameter sensitivity for the current wavelengths at small optical thicknesses.

Future work will also center on examining any potential correlation between cloud top particle size and rain rate in both water and ice clouds, as well as comparisons between the VIRS retrieved liquid water path and other data sources.

Theoretical analysis will be performed on synthetic clouds to determine the intra-cloud weighting functions of a variety of near-IR channels (e.g. 1.63 and 3.75 microns) in order to assess the degree to which different channels contain physically distinct information. This work could lead to the retrieval of a crude vertical profile of particle sizes within the upper reaches of water clouds.

Finally, an initial look at the aerosol indirect effect was compelling in a seasonally averaged sense. Future work will examine the correlation between boundary layer aerosol optical thicknesses with collocated cloud top effective radius retrievals. This will be soon be possible utilizing the instrument array available on the A-train.

REFERENCES

Bennedetti, A., P. Gabriel, and G. L. Stephens: 2001, Properties of reflected sunlight derived from Green's function method. *Journal of Quantitative Spectroscopy and Radiative Transfer,* **72,** 201-225

Boers R.: 1997, Microphysical and short-wave radiative structure of stratocumulus clouds over the Southern Ocean: Summer results and seasonal differences. *Quarterly Journal of the Royal Meteorological Society*,**124**,151-168

Cess, R.D., G.L. Potter, J.P. Blanchet, G.J. Boer, S.J. Ghan, J.T. Kiehl, H. Le Truet, Z. X. Li, X. Z. Liang, J.F.B. Mitchell, J.J. Morcrette, D.A. Randall, M.R. Riches, E. Roeckner, U. Schleses, A. Slingo, K. E. Taylor, W.M. Washington, R.T. Wetherald and I. Yagai: 1989, Interpretation of cloud-climate feedback as produced by 14 atmospheric general circulation models. *Science,* **245,** 513-516

Chen, C.T. and V. Ramaswamy: 1996, Sensitivity of Simulated Global Climate to Perturbations in Low-Cloud Microphysical Properties. Part I: Globally Uniform Perturbations. *Journal of Climate*: **9**, pp. 1385–1402.

Eriksson, P.: 2000, Analysis and comparison of two linear regularization methods for passive atmospheric observations, *Journal of Geophysical Research,* **105,** 18157-18167

Gabriel, P., M. Christi, and G.L. Stephens: 2005, Calculation of Jacobians for inverse radiative transfer: An efficient hybrid method. *Journal of Quantitative Spectroscopic Radiative Transfer, To be submitted.*

Gabriel, P. and M. Christi: 2004, RADIANT Version 2.0 users guide.

Han, Q., W.B. Rossow, and A.A. Lacis: 1993, Near-global survey of effective droplet radii in liquid water clouds using ISCCP data. *Journal of Climate*, **7,** 465-497

Juliette, H. L. and C. Clerbaux: 1999, An inversion algorithm using neural networks to retrieve atmospheric co total columns from high-resolution nadir radiances. *Journal of Geophysical Research*, **104,** 23841-23854

King M.D and Harshvardhan: 1986, Comparative accuracy of selected multiple scattering approximations. *Journal of the Atmospheric Sciences,* **43,** 784-801

King M.D., Y.J. Kaufman, W. P. Menzel, and D. Tanre: 1999, Remote sensing of cloud, aerosol, and water vapor properties from the Moderate Resolution

McClatchey R.A., R.W. Fenn, J.E.A. Selby, F.E. Volz, and J.S. Garing: 1972, Optical properties of the atmosphere. Air Force Cambridge Research Laboratories, AFCRL-72-0497, Environmental Research Paper, No. 411, 108 pp.

Marks, C.J. and C.D. Rodgers: 1993, A retrieval method for atmospheric composition from limb emission measurements. *Journal of Geophysical Research,* **98,** 14939-14953.

Nakajima T. and T. Nakajima: 1995, Wide area determination of cloud microphysical properties from NOAA AVHRR measurements from the FIRE and ASTEX regions. *Journal of the Atmospheric Sciences,* **52,** 4043-4059

Nakajima, T. and M.D. King: 1990, Determination of the optical thicknes and effective particle radius of cloud from reflected solar radiation measurements. part I: Theory. *Journal of the Atmospheric Sciences,* **47,** 1878-1893.

Platnick S.: 2000, Vertical photon transport in cloud remote sensing problems. *Journal of Geophysical Research.* **105,** 22919-22935

Platt C.M.R.: 1973, Lidar and radiometric observations of cirrus clouds. *Journal of the Atmospheric Sciences,* **30,** 1191-1204

Ramanathan, V.: 1981, The Role of Ocean-Atmosphere Interactions in the CO2-Climate Problems. *Journal of the Atmospheric Sciences*, **38,** 918-930.

Ramanathan, V.: 1987, The Role of Earth Radiation Budget Studies in Climate and General Circulation Research. *Journal of Geophysical Research*, **92,** 4075-4095.

Ramanathan, V., E. F. Harrison, and B. R. Barkstrom: 1989, Climate and the Earth's Radiation Budget. *Physics Today*, **42,** 22-33.

Rodgers, C.D.: 1976, Retrieval of atmospheric temperature and composition from remote measurements or thermal radiation. *Review of Geophysics and Space Physics,* **14**, 609-624.

Rodgers, C.D.: 1990, Characterization and error analysis of profiles retrieved from remote sounding measurements. *Journal of Geophysical Research,* **95,** 5578-5595.

Rolland, P., K.-N. Liou, M.D. King, S.-C. Tsay, and G.M. McFarquhar: 2000, Remote sensing of optical and microphysical properties of cirrus clouds using Moderate Resolution Imaging Spectroradiometer channels: Methodology and sensitivity to physical assumptions. *Journal of Geophysical Research,* **105,** 11721-11738.

Rosenfeld D. and I. Lemsky: 1998, Space-Borne based insights into precipitation formation processes in continental and maritime convective clouds. *Bulletin of the American Meteorological Society*, **79**, 2457–2476.

Rossow, W.B., A.W. Walker, and L.C. Garder: 1993, Comparison of ISCCP and other cloud amounts. *Journal of Climate*, **6**, 2394-2418.

Tamminen, J. and E. Kryola: 2001, Bayesian solution for nonlinear and non-gaussian inverse problems by Markov chain Monte Carlo method. *Journal of Geophysical Research,* **106,** 14377-14390.

Tanre, D., M. Herman, and Y.J. Kaufman: 1996, Information on aerosol size distribution contained in solar and reflected spectral radiances. *Journal of Geophysical Research,* **101,** 19043-19060.

Twomey, S.: 1980, Cloud nucleation in the atmosphere and the influence of nucleus concentration levels in atmospheric physics. *Journal of Physical Chemistry,* **84,** 1459-1463.

Twomey, S and T. Cocks: 1982, Spectral reflectance of clouds in the near-infrared. Comparison of measurements and calculations. *Journal of the Meteorological Society of Japan,* **60,** 583-592

Van de Hulst H. C.: 1980, *Multiple Light Scattering*, volumes 1-2. Academic Press, New York.

Weatherald, R. T., and S. Manabe: 1988, Cloud feedback processes in a general circulation model. *Journal of the Atmospheric Sciences,* **45,** 1397-1415.

Worden, J. R., K. W. Bowman, and D. B. Jones: 1999, Two-dimensional characterization of atmospheric profile retrievals from limb sounding observations. *Journal of Quantitative Spectroscopic Radiative Transfer,* **86,** 45-71.